

AD-764 904

IR WINDOW STUDIES

F. A. Kroger, et al

University of Southern California

Prepared for:

Air Force Cambridge Research Laboratories
Advanced Research Projects Agency

15 December 1972

DISTRIBUTED BY:

NTIS

National Technical Information Service
U. S. DEPARTMENT OF COMMERCE
5285 Port Royal Road, Springfield Va. 22151

Reproduced by
NATIONAL TECHNICAL
INFORMATION SERVICE
U.S. Department of Commerce
Springfield VA 22151



UNIVERSITY OF SOUTHERN CALIFORNIA

IR WINDOW STUDIES

F. A. Kroger and John H. Marburger

Contract No. F19628-72-C-0275

Quarterly Technical Report No. 2
15 December 1972

Contract Monitor: Alfred Mahan
Solid State Sciences Laboratory

Approved for public release; distribution unlimited.

Prepared for the Defense Advanced Research Projects Agency

ARPA Order No. 2055, as Monitored by
AIR FORCE CAMBRIDGE RESEARCH LABORATORIES
AIR FORCE SYSTEMS COMMAND
UNITED STATES AIR FORCE
BEDFORD, MASSACHUSETTS 01730

ELECTRONIC SCIENCES LABORATORY

IR WINDOW STUDIES

by

F. A. Kroger

and

John H. Marburger

**Electronic Sciences Laboratory
School of Engineering
University of Southern California
Los Angeles, California 90007**

Contract No. F19628-72-C-0275

**Quarterly Technical Report No. 2
15 December 1972**

**Contract Monitor: Alfred Kahan
Solid State Sciences Laboratory**

Approved for public release; distribution unlimited.

Prepared

for

**Sponsored by
Defense Advanced Research Projects Agency
ARPA Order No. 2055**

**Monitored by
AIR FORCE CAMBRIDGE RESEARCH LABORATORIES
AIR FORCE SYSTEMS COMMAND
UNITED STATES AIR FORCE
BEDFORD, MASSACHUSETTS 01730**

Unclassified

DOCUMENT CONTROL DATA - R & D		
<i>(Security classification of title, body of abstract and indexing annotation must be entered when the overall report is classified)</i>		
1. ORIGINATING ACTIVITY (Corporate author) Electronic Sciences Laboratory University of Southern California Los Angeles, California 90007		2a. REPORT SECURITY CLASSIFICATION UNCLASSIFIED
2b. GROUP		
3. REPORT TITLE IR WINDOW STUDIES		
4. DESCRIPTIVE NOTES (Type of report and inclusive dates) Scientific. Interim.		
5. AUTHOR(S) (First name, middle initial, last name) F. Kroger and John H. Marburger		
6. REPORT DATE 15 December 1972	7a. TOTAL NO. OF PAGES 70	7b. NO. OF REFS 19
8a. CONTRACT OR GRANT NO F19628-72-C-0275	8b. ORIGINATOR'S REPORT NUMBER(S) USCEE Report No. 443	
8c. PROJECT XX , Task, Work Unit Nos. DodElement 6110D	8d. OTHER REPORT NO(S) (Any other numbers that may be assigned this report) AFCRL-TR-73-0054	
8d. Dod Subelement n/a		
10. DISTRIBUTION STATEMENT A - Approved for public release; distribution unlimited		
11. SUPPLEMENTARY NOTES Tech, TECH, OTHER	12. SPONSORING MILITARY ACTIVITY Air Force Cambridge Research Laboratories (LQ) L. G. Hanscom Field Bedford, Massachusetts 01730	
13. ABSTRACT <p>During this quarter advances have been made in the theory of multiple phonon absorption mechanisms, the theory of thermal skewing of asymmetric beams, and in the experimental characterization of IR window materials. Preliminary calorimetric measurements of the absorption coefficient in melt grown chromium-free GaAs versus wavelength yield values lower than any previously measured in chromium doped samples. The results of measurements of the mechanical properties of GaAs, and data related to the defect chemistry of CdTe and CdS are also reported. Systems for the production of ultra pure alkali halide and III-V compounds are nearing completion.</p>		
14. Keywords: IR Windows, Alkali Halides, III-V Semiconductors, II-VI Semiconductors, Thermal lensing, IR absorption.		

DD FORM 1 NOV 68 1473

00
li
BT

Security Classification

ABSTRACT

During this quarter advances have been made in the theory of multiple phonon absorption mechanisms, the theory of thermal skewing of asymmetric beams, and in the experimental characterization of IR window materials. Preliminary calorimetric measurements of the absorption coefficient in melt grown chromium-free GaAs versus wavelength yield values lower than any previously measured in chromium doped samples. The results of measurements of the mechanical properties of GaAs, and data related to the defect chemistry of CdTe and CdS are also reported. Systems for the production of ultra pure alkali halide and III-V compounds are nearing completion.

CONTENTS

	Page
ABSTRACT	1
1. INTRODUCTION	3
2. PROGRESS BY PROJECT	
a. 1 Effect of Oxygen and Other Impurities on IR Absorption in II-VI and III-V Compounds	4
a. 2 Optimization of Alkali Halide Window Materials	7
a. 3 Growth of Crystals for IR Window Research	12
b. 1 Fabrication of Polycrystalline IR Window Materials	17
c. 1 Mechanical Behavior of III-V and II-VI Compounds	21
d. 1 Surface and Interface IR Absorption	30
d. 2 Study of Defects in II-VI Compounds	32
e. 1 Theoretical Studies of Absorption Mechanisms in IR Window Materials	37
f. 1 Techniques for Indirect Measurement of Small Absorptive Losses	50
g. 1 Characterization of Optical Performance of IR Window Systems	55
3. DISCUSSION	65
4. SUMMARY	66

1.

INTRODUCTION

The format of this report follows closely that of the first quarterly report in which projects are identified by codes keyed to the contract work statement.

The various categories are briefly

- a) Crystal growth
- b) Polycrystalline window fabrication
- c) Mechanical properties of window materials
- d) Window material defect characterization
- e) Theory of residual IR optical absorption
- f) Absorption measurement techniques
- g) Theoretical evaluation of optical performance of windows

The most important projects in areas a) and b) require facilities which did not exist at USC prior to this contract, and consequently progress in these areas is initially slower than in the others. Projects c) through g) have yielded data during this period which are reported in the corresponding project reports.

a. 1. Effect of Oxygen and Other Impurities on IR Absorption in
II-VI and III-V Compounds

J. M. Whelan, M. Gershenzon

Absorption coefficient data in the 10.6 μm wavelength region for GaAs are primarily based on GaAs samples made semi-insulating by doping with Cr during growth from near stoichiometric melts. Such samples must be viewed with caution as being representative of better quality high resistivity GaAs which can be prepared in moderate yields. Reasons for this position are the low or non-measurable Hall mobilities in most Cr doped crystals. This is an almost certain indication of inhomogeneities in such samples. Semi-insulating GaAs crystals prepared by oxygen doping, or unintentionally doped, and grown under conditions in which the Si contamination should have been small, have had significantly high Hall mobilities in the 2000-7000 $\text{cm}^2 \text{v}^{-1} \text{s}^{-1}$ range at room temperature with corresponding electron concentrations of 10^7 - 10^8cm^{-3} . Within this class of samples there are marked variations in secondary electrical characteristics such as trapping times which are indicative of varying deep impurity levels. These can contribute to IR absorption. Because the number of laboratories doing substantial amounts of work on semi-insulating GaAs has markedly decreased in the past five years, there is a general consensus that the availability of "selected high quality" semi-insulating GaAs has also declined. In order to increase the scope of GaAs samples which might contribute to a more definitive evaluation of GaAs as a window material, a search has begun to locate remaining samples of GaAs prepared within the past 10 years which were judged to be good in an electrical sense. The willingness of individuals contacted to cooperate has been excellent. Results of this activity will be available shortly.

Progress on several projects described below are noted in this report because of their relevance to the IR Window effort although

they are not funded by that program. The first of these is the development of a method for measuring the concentrations of oxygen in GaAs, which can be extended to other semiconductors and possibly salts. Oxygen in GaAs is an important dopant or getter for GaAs because crystals grown in oxygen-containing environments can be made semi-insulating with high mobilities (as contrasted with Cr doped crystals). The longest trapping times reported for bulk GaAs were in an oxygen doped crystal. The GaAs sample with the lowest β measured at U.S.C. in the 10.6 μm region was oxygen doped. At present there is no reliable method to measure the oxygen concentration. Our proposed method is to measure the oxygen fugacity in a metallic solution before and after dissolving a known amount of GaAs, by measuring the emf of a solid oxygen ionic conductor used as a concentration cell (stabilized zirconia in our case). Required information for this procedure is the dependence of the fugacity on oxygen concentration. For Ga solutions at 500°C the preliminary relationship between the fugacity of $\text{O}_2(\text{g})$ and the corresponding equilibrium mole fraction of O in Ga is : $X(\text{O in Ga solu.}) = 6 \times 10^{17} f(\text{O}_2, \text{g})$. This applies for mole fractions of oxygen of 10^{-7} or less. The oxygen fugacity of dissolved oxygen for $X(\text{O in Ga solu.}) = 10^{-7}$ is approximately five orders of magnitude below that which can be achieved by equilibrating Ga with $\text{H}_2(\text{g})$ containing only 1 ppm of H_2O at 500°C. This program grew out of an original effort to grow GaAs epitaxial films with low oxygen concentrations and at lower temperatures than nominally used. It is planned to complete the original goal within the next reporting period. Such films will be made available for evaluation of deep levels by Professor Crowell using variable frequency capacitance measurements.

A horizontal epitaxial solution growth epitaxial system for GaAs is nearing completion. It will utilize our approach to growing films with controlled oxygen concentrations without the necessity of using

commercial stabilized zirconia or thoria tubes. Such tubes are relatively impure and may be expected to contaminate the GaAs to some yet unknown degree.

Another program recently started which is related to the window program is the development of a novel method for growing bulk GaAs under a semi-permeable membrane which passes arsenic but not Si or O. These features should enhance the control for doping with Cr and reduce the amount of Cr needed. Under usual conditions Cr doping control is complicated by oxidation of the Cr and variable amounts of Si contamination.

a.2. Optimization of Alkali Halide Window Materials

P. J. Shlichta, R. E. Chaney

Status of Program: The principal objective of this part of the program is the determination of the effect of impurities and lattice defects on the mechanical and optical properties of KCl and other alkali halides. This will be accomplished by growing and testing crystals both of the highest possible purity and with known impurities. As of the present quarter, the solution purification apparatus is operational, the purification-growth chamber is assembled, and the gas treatment apparatus is being assembled. Under present schedules, high-purity KCl crystals should be in production by the end of January. Arrangements have been made for calorimetric absorption measurements at USC of crystals from other laboratories and for sending USC-grown crystals to other laboratories for testing.

Purification and Growth of KCl Crystals:

As has been described in the previous quarterly report (1), KCl is being purified by a modification of the procedure of Fredericks, Schuerman, and Lewis (2, 3). Reagent-grade starting material is purified by (A) dissolution in water and successive passage through cation- and anion-exchange resins, (B) fractional crystallization, (C) melting and treatment with Cl_2 and HCl (and/or CCl_4) to remove volatile anionic impurities.

- (A) The flow system for the ion exchange apparatus is essentially the same as that of Fredericks et al (Figure 4 of ref. 3) with the addition of a final passage through a Millipore filter. The cationic and anionic resins are Chelex 100 and AGX 100 respectively; both are from Bio Rad Laboratories. The water used for all solution and rinsing operations is deionized by passage through BioRad AG 501-X8 (D) resin. This system is now operational.
- (B) The purified KCl solution is heated to about 80-90°C and evaporated, under aspirator vacuum, until the first crystals form. Since these usually form around solid nuclei (e. g. dust) and since the first fraction of crystallization tends to sequester heavy

metal ions such as Pb^{++} and Cd^{++} (4), the solution is refiltered and the crystals dissolved and recycled to (A). The solution is then further evaporated until about 75% of the solute has crystallized out. The remaining solution is discarded. The moist crystals are then, with or without further drying, transferred to crucibles for further treatment.

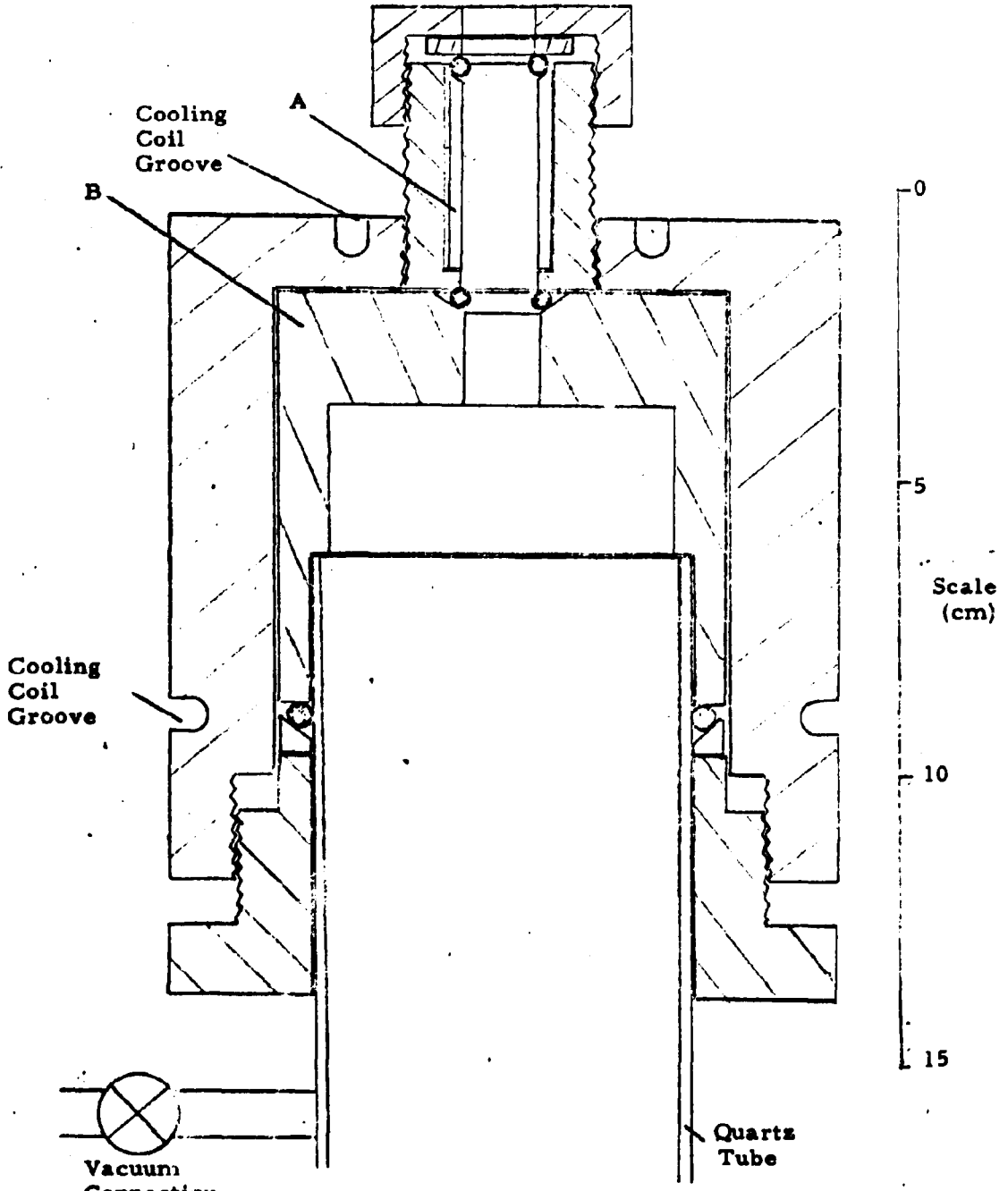
Work on this stage of purification has just begun. Since the danger of airborne contamination is greatest during these operations, attempts are being made to construct special plastic containers which will make external transfer unnecessary. Cleaning of the crucibles and transfer of the purified salt into the crucibles will be carried out in a laminar-flow clean bench.

- (C) The purified salt, packed into vitreous carbon or pyrographite crucibles, is placed in a purification-growth chamber in which all subsequent operations (gas treatment, fractional distillation and crystal pulling) are performed. This chamber consists of a fused silica tube 64 mm O. D. and 600 mm long, closed off at the bottom and sealed at the top by a composite end-seal (Figure 1). This device provides water-cooled o-ring seals between the silica tube and pull rod (or gas-inlet tube) without the introduction of any contaminative (i. e. metallic) parts into the purification-growth chamber. Moreover the interchange of liners permits accommodation of a variety of tube diameters. Future plans call for mounting a vacuum ball valve and second O-ring seal on top of the present end seal so that pull rods and gas-inlet tubes can be easily interchanged and so that a succession of crystals can be grown without disturbing the melt or chamber atmosphere.

The gas-treatment apparatus is now being assembled and should be ready by the end of the month. The crystal puller is operational, although some improvements are being considered. The crystal-puller furnace and temperature control will be assembled by the end of January.

Evaluation of Available Crystals: Since the USC infrared calorimeter is now operational (see section f.1) it has been proposed that, pending the availability of USC-grown crystals, preliminary absorption measurements might be made upon presently available crystals, either from previous work of the present investigators or from other sources. It is our belief that such measurements are of value only when made on as-grown crystals of specially purified material. Accordingly, arrangements for the exchange of "highest purity" crystals have been made between the present investigators, Prof. W. Fredericks (Oregon State University), and Prof. W. Sibley (Oklahoma State University). Samples from Prof. Fredericks have already been received and results of calorimetric measurements will probably be included in the next quarterly report.

It is very doubtful, however, whether there is any advantage to making measurements on commercial or impurity-doped crystals from outside sources. This is partly because the variety of techniques used for purification, crystal growth, and sample preparation result in significant variations in the concentrations of known and unknown impurities. Moreover, since the physical state of a given impurity may be profoundly modified by annealing or by interaction with dislocations or vacancies, the optical and mechanical properties of a specimen are often dependent upon its thermal and mechanical history. Thus, the infrared spectra of sulfate ion in KCl depends not only upon the presence or absence of divalent cations, but also upon whether the specimen has been recently quenched or allowed to anneal at room temperature (5). It has also been shown that the storage of cleaved samples, for several months, in non-evacuated bottles can cause hydroxide contamination from atmospheric moisture (6). Similarly, even slight deformations of as-grown crystal rods can cause rapid atmospheric contamination and consequent embrittlement (7). For these reasons, in the present project, measurements of the optical and mechanical properties of impurity-doped alkali halides will be carried out only on as-grown crystals for which every step of preparation is known and can be evaluated.



End Seal of Purification-Growth Chamber
 All parts are anodized aluminum except a and b
 which are either Teflon or impervious carbon.

Figure 1

REFERENCES

1. Marburger, John H., et al. Electronic Sciences Laboratory, University of Southern California, "IR Window Studies," Quarterly Technical Report No. 1 (June-August 1972), Contract No. F19628-72-C-0275, ARPA Order No. 2055 (29 September 1972).
2. Fredericks, W. J. et al. "An Investigation of Crystal Growth Processes." Grant No. AF-AFOSR 217-63. Project Task: 9762-02 Solid State Sciences Division, Air Force Office of Scientific Research, Washington, D. C. (January 1966).
3. Rosenberger, F. "Purification of Alkali Halides" to be published in Techniques of Ultrapurity, M. Zief and B. Speights (editors), Marcel Dekker.
4. Glasner, A., Israel J. Chem. 7, 649, 657 (1969).
5. Decius, J. C., Cober, E. H., and Brenna, G. L., Spectrochimica Acta 19, 1281-1289 (1963).
6. Chaney, R. E. and Fredericks, W. J., J. Phys. Chem. Solids (in press).
7. Shlichta, P. J., "Effect of Predeformation on the Mechanical Properties of Sodium Chloride Crystals," JPL Technical Report No. 32-923, Jet Propulsion Laboratory, (May 1, 1966).

a. 3. Growth of Crystals for IR Window Research

E. A. Miller and W. R. Wilcox

(Chemical Vapor Deposition of Bulk Gallium Arsenide Crystals)

Our working hypothesis is that melt growth is incapable of producing low absorptivity gallium arsenide because of attack of crucible materials and high solubility of impurities at the high temperatures required. As an alternative, two chemical vapor deposition methods are being investigated: (a) transport in a close system and (b) deposition in a flow-through system (as normally used for preparation of thin films).

During this reporting period most of our effort was devoted to construction of the flow-through system.

1. Growth in a Sealed Tube on an Internal Projection

As reported previously, polycrystalline growth occurs in the tapered seed zone during iodine transport of GaAs in a temperature gradient. It seemed likely that less nucleation would be produced if crystals could be induced to grow on a small internal projection rather than on the walls of the tube. In attempting to accomplish this, an air stream was directed into an internal projection consisting of a 1 mm quartz capillary capped with a 1 mm thick quartz disc. The capillary projected about 5 mm into the 10 mm I. D. quartz growth tube. After several trials a ~ 0.3 mm faceted crystal was obtained. Reinsertion of this tube into the furnace for two days produced clusters of polycrystalline overgrowths. Best results were obtained when the temperature of the vapor space was higher than both feed and growing crystals.

Another projection tested was an inserted tube open at the other end to act as a radiation pipe. Growth occurred between the tip of this projection and the end of the tube, rather than on the tip.

2. Travelling Heater Vapor Growth Method

In this technique a short vapor zone is moved slowly through solid GaAs by lowering the tube through a short heater. A maximum temperature is produced thereby in the vapor zone, to eliminate the deleterious effects of constitutional supercooling. Furnaces were constructed with a single-turn heating element wrapped around an alumina or quartz tube of slightly larger diameter than the 10 mm O. D. quartz tube containing the GaAs. The heater was made of Kanthal wire wound in a tight helix of about 4mm diameter. The heater was then surrounded by bubbled alumina insulation to produce a temperature gradient of about $8^{\circ}\text{C}/\text{mm}$ in the furnace adjacent to the crystal. A 15 mm long polycrystalline ingot was obtained at a travel rate of 5 mm/day. The interface was rough, presumably due to constitutional supercooling. Therefore a furnace with about twice the temperature gradient was constructed by omitting the insulation about the heater tube and mounting the heating element immediately adjacent to the tube containing the GaAs. At a travel rate of ~ 1 mm/day no growth was obtained, presumably because of condensation in the cold vapor spaces alongside the feed. In the future it will be necessary to prepare feed that fills the tube.

3. Carbon Coating of Tube Wall

In order to minimize nucleation and adhesion of growing crystals to the wall of the tube, some tubes were coated internally with a film of carbon. The carbon was deposited by pyrolytically decomposing acetone vapors in a helium stream at temperatures in excess of 950°C . Tests were run with both travelling heater and internal projection tubes. In some cases, results were favorable. In general, overall adhesion was reduced except in the few spots where the coating failed, and there the adhesion was quite strong. Individual crystal size did not improve

significantly based on the few tests run.

4. Open Tube CVD Facility

The construction of this facility consumed most of our effort during this quarterly period. Since some of the gases to be handled in this process are highly toxic, the complete facility was enclosed in a 12' long x 6½' high x 3' deep hood. Clear acrylic panels were fastened to the outside frame. One section in the front will have sliding doors for access. Two exhaust lines were provided: one for the overall hood volume, and a second for the exhaust gas burn off area.

The all stainless steel piping was completed for each of the various transport methods planned for study as shown in Figure 1. A separate line leading off a common hydrogen manifold goes through the appropriate flowmeter to each materials source. Sources include: 1) AsCl_3 bubbler, 2) AsCl_3 bubbler with bypass and reduction furnace to produce high purity HCl at low concentration, 3) Trimethyl gallium bubbler, 4) H_2 flush for reaction tube, 5) H_2 for varying the mixing ratio in the mixing manifold, 6) AsH_3 in H_2 , and 7) pure anhydrous HCl. Means were also provided for introducing HCl in the reactor to minimize extraneous GaAs deposition on the walls.

5. Future Work

During the next quarter, the open tube CVD system will continue to be emphasized. We plan to have it in operation by December 15, 1972. The first transport system planned for study is the AsCl_3 -Ga- H_2 method, which offers greater reliability because its few starting components can be obtained in high purity. Next the AsH_3 -(CH_3)₃Ga- H_2 system is planned for investigation. Finally the As-Ga-HCl- H_2 system will be studied (with this system the Ga to As ratio can be varied).

Work with the travelling heater method will be directed toward solving the problem of condensation of the transporting species. If time allows, some effort will also be devoted to work on the internal projection stationary tube. We will attempt to develop a furnace permitting observation of the tube during growth. Evacuation of the tubes down to a high vacuum of 10^{-6} to 10^{-7} torr prior to sealing is planned. Up to now the vacuum produced prior to sealing has only been in the region of 10^{-3} torr.

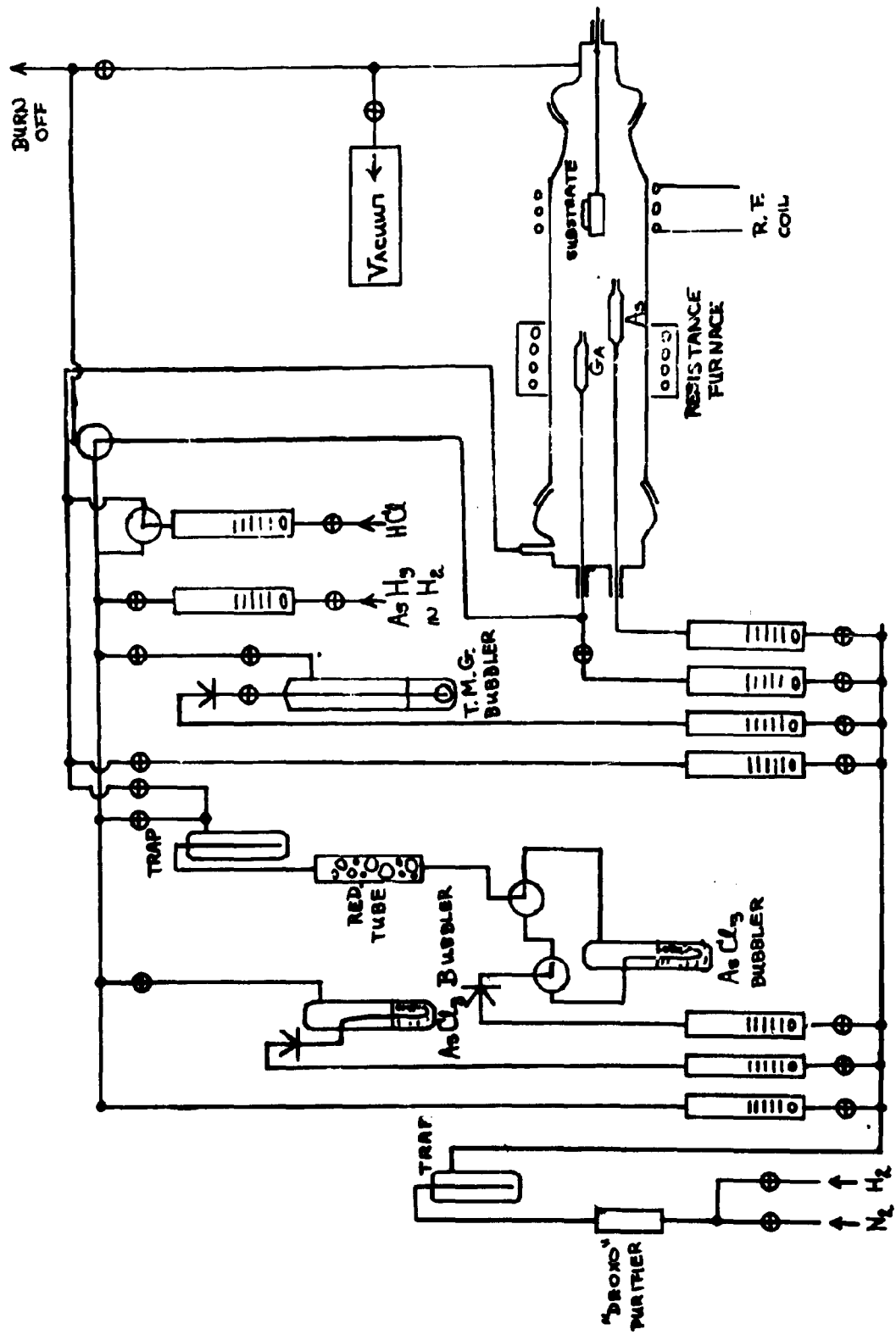


Fig. 1

b. 1. Fabrication of Polycrystalline IR Window Materials

S.M. Copley, J.M. Whelan, V. Rana, G. Berkstresser

This part of the program is concerned with producing polycrystalline gallium arsenide samples by hot pressing the gallium arsenide powder in the presence of a volatile sintering aid. By this novel technique it should be possible to enhance the purity and control the grain size of the samples so as to yield a high performance IR window material. The same technique can be used for other semiconducting compounds, including the II-VI family.

Working drawings of the hot press and the operating procedure were given in the previous quarterly report. This hot press has now been fabricated at the U.S.C. Engineering Machine Shop. Figure 1 shows the hot press assembly. This hot press will soon be ready for operation.

During hot pressing excess arsenic will be utilized as a sintering aid. The vapors of arsenic will be contained in the die (G) by pressurizing the hot press chamber with argon and employing a molten glass seal (E).

For hot pressing, the die (G), Fig. 2, will be loaded with gallium arsenide powder. Chips of glass will be placed in the recess at the top, between the die and the die plunger (H). This die will then be installed inside the furnace chamber (F), as shown in Fig. 3., and the hot press chamber (D) will be evacuated. The gallium arsenide powder will then be compressed by transmitting the pressure of the diaphragm pressure cylinder (A) to the die plunger (H) via a pressure ram foot (B) and a load ram (C). Furnace (F) will then be heated to melt the glass at the top. The chill (I) will also be started at the same time so as to keep the powder with excess arsenic at a lower temperature (below 250°C). When the glass is molten and forms a seal at the top, the chamber (D) will be pressurized with Argon. The chill will be turned off and the temperature of the furnace raised

to the desired value.

The function of arsenic during hot pressing is to facilitate the rearrangement of the particles.

After compaction the chamber (F) will be allowed to cool, while the load and the pressure of Argon will be removed. After cooling the compact will be removed from the hot press. Annealing of this compact will be done to remove the excess arsenic and also to increase the densification further.

The diameter of the compacts obtained from this press will be 1/2". This press has the pressure capability to 5000psi (on the compact) and temperature capability to 1200°C, at present.

In the next quarterly period preliminary experiments will be carried out to demonstrate the effectiveness of this technique. Initial efforts will be concerned with determining the factors affecting the quality of the hot pressed material.

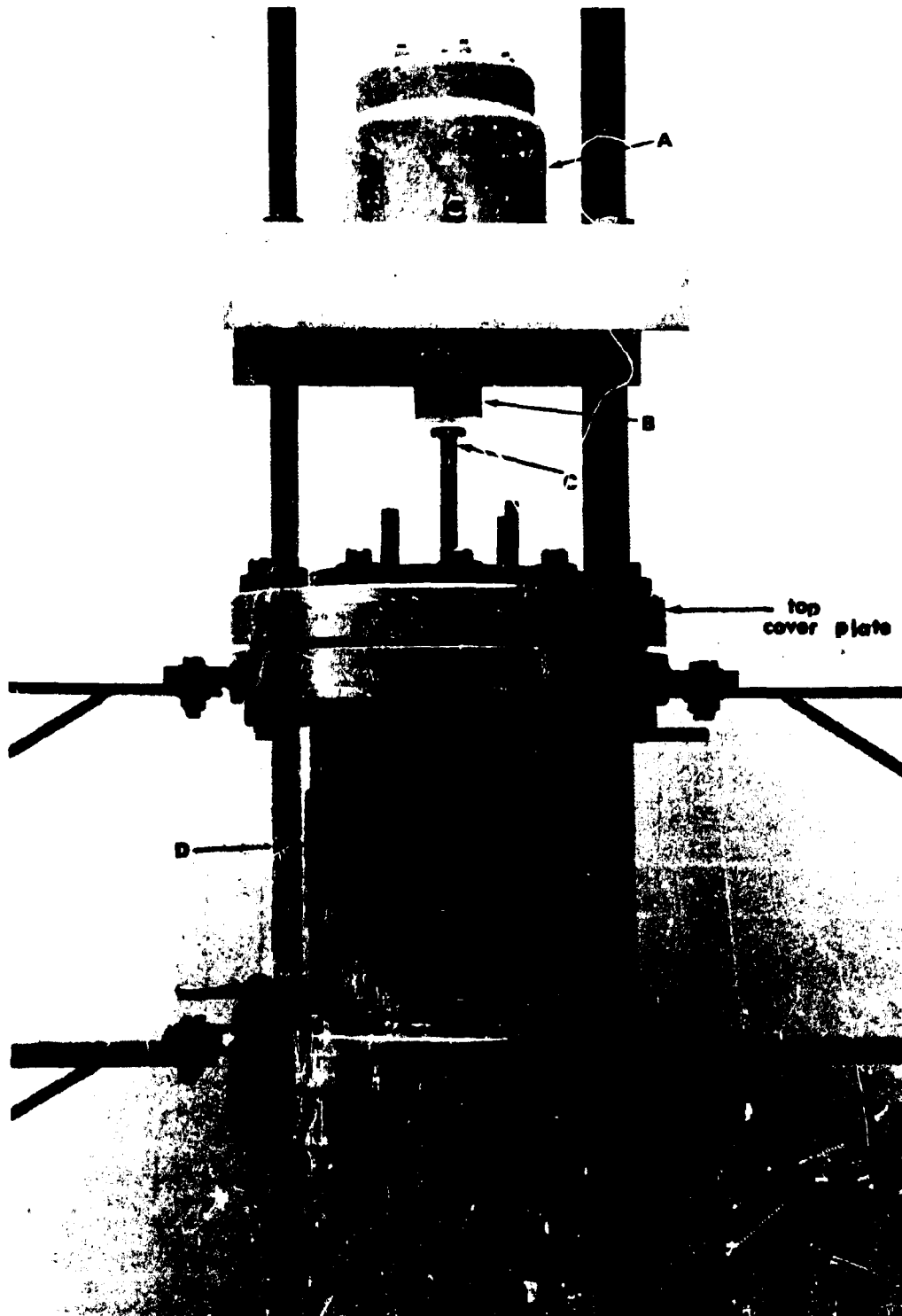


Fig. 1: Hot Press Assembly

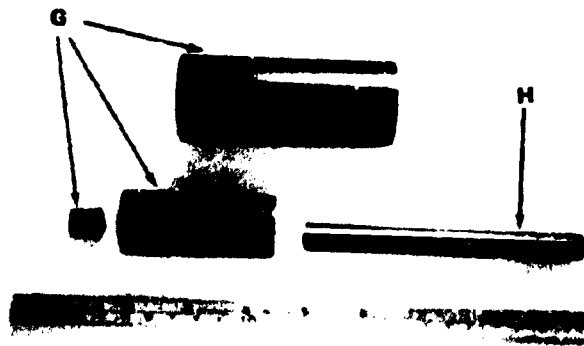


Fig. 2. Hot Press Die and Plunger

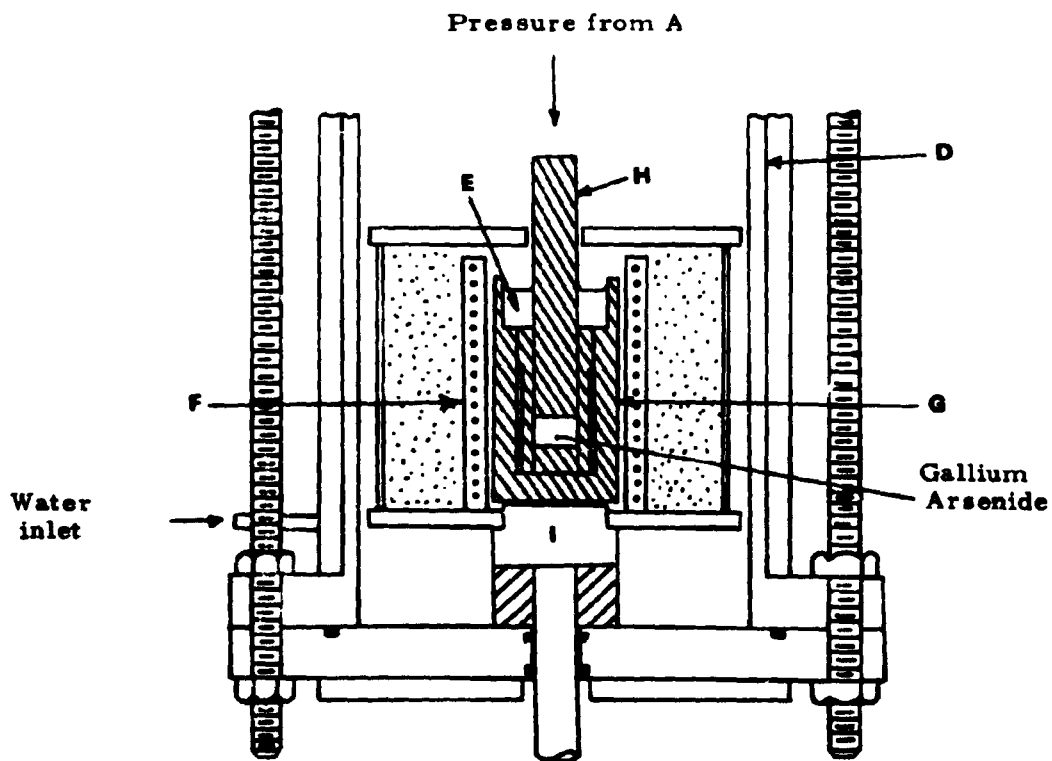


Fig. 3: Set Up Inside the Hot Press Chamber

c. 1. Mechanical Behavior of III-V and II-VI Compounds

S.M. Copley, V. Swaminathan, V. Rana

This investigation is concerned with a determination of the mechanical behavior of various window candidate materials. A study of the mechanical behavior of single crystals of GaAs doped with Si has been initiated.

A 350 gm melt grown single crystal of Si-doped GaAs with a carrier concentration of $1.8 \times 10^{18}/\text{cm}^3$, a mobility of $1900 \text{ cm}^2/\text{v. sec}$ and a resistivity of $1.89 \times 10^{-3} \Omega \text{ cm}$ was obtained from Crystal Specialties, Inc. *. Compression specimens with different length to width ratios were prepared by a series of operations including initial shaping with a precision cut-off wheel, two-circle goniometer unit to give selected orientations and precision grinding. Specimens with $\langle 100 \rangle$ and $\langle 111 \rangle$ stress axes were selected for the initial stress-strain experiments on the basis of Schmid factor considerations. The $\langle 100 \rangle$ stress axis favors slip on $\{111\} \langle 1\bar{1}0 \rangle$, the previously observed slip system (1), while the $\langle 111 \rangle$ stress axis favors slip on other systems.

Characterization of the Structure: Successful etching techniques have been developed to measure the dislocation density prior to deformation. Wafers with A(111) orientation were cut and the surfaces of these wafers were lapped and polished with 600 grit silicon carbide powder with water as lubricant. After being rinsed with deionized water, they were chemically polished in a slowly stirred solution of $3\text{H}_2\text{SO}_4 - 1\text{H}_2\text{O}$ for 5-10 minutes at $50-55^\circ\text{C}$ (2). The etching experiments were carried out at room temperature (warming up the solution increases the etching rate). The etchant employed was $1\text{HNO}_3 - 3\text{H}_2\text{O}$ (3). Samples were etched for at least 15 minutes. Figure 1 shows the etch figures obtained on an A(111) face and on another oblique (111) face. From the photo-micrographs the dislocation density was measured as $9.0 \times 10^4/\text{cm}^2$.

* Crystal Specialties, Inc., 419 W. Maple, Monrovia, California 91016

Electron Microscopic Studies: The transmission electron microscope is a very useful instrument for characterizing both the as grown and deformed structure of any material. However, in order to observe the structure of a material under the electron microscope one must be particularly concerned with its electron transparency. One needs specimens on the order of 1000 Å thick or less for observation of structure by electron transmission. Hence, preparing such thin specimens is a very difficult task especially for a brittle material like GaAs.

A successful jet polishing technique has been developed for preparing thin foils of GaAs. This technique is a modification of a previously described technique used for preparing thin films of GaAs (4). A schematic diagram of the apparatus is shown in Fig. 2. The advantage of using a jet polishing technique is that one can start with a thicker specimen than is needed for other conventional specimen preparation techniques. Since GaAs cleaves easily, one can obtain slices of 1/8 inch diameter and 0.010 inch thick, as the starting specimen. An impression is chemically polished in the sample, and the disk is turned over and polished from the second surface so that two impressions meet in the center of the disk. The formation of a small hole is observed visually by the light transmitted through the disk. Regions near the hole periphery are suitable for examination.

Several polishing solutions have been tried. A solution of $5\text{HNO}_3-2\text{HF}-1\text{HCl}-6\text{H}_2\text{O}$ was tried first. Due to the severe attack of HF on GaAs, the observation of the structure was obscured by excessive accumulation of dirt which maybe precipitates of gallium fluoride. The solution that is currently used is $4\text{HCl}-4\text{H}_2\text{O}_2-1\text{H}_2\text{O}$. Typical microstructures observed under the microscope are shown in Figs. 3 and 4.

Figure 3a shows what appears to be a network of dislocations with precipitates on them; however, the lines do not go in and out of

contrast systematically when the foil is tilted as they should if they were really to be dislocations. Therefore, it appears that this type of contrast may be due to some kind of artifact.

Figure 3b shows electron micrographs of multilayer stacking faults which have previously been observed by Laister et. al. (5).

Figure 4 shows an electron diffraction pattern from a Si-doped GaAs specimen. Of particular interest are the extra spots and heavy streaks in the pattern. These observations confirm previous observations by Meieran (4). The presence of these extra spots and streaks has yet to be explained satisfactorily.

Stress-Strain Tests: It is well known that semiconducting materials though brittle at room temperature deform plastically at temperatures greater than $0.5 T_m$ where T_m is the melting point in degree Kelvin. Previous study of mechanical behavior of GaAs was carried out at 500°C on single crystals with (111) stress axis in compression (1). In the present investigation, the first stress-strain experiment was performed at 500°C in compression on a sample with length to width ratio of 1.5 and with a stress axis of $\langle 100 \rangle$. The compression test was carried out at a constant force rate. A constant force rate experiment is one in which the specimen is loaded by increasing the force acting on it at a constant rate. The difference between the true applied stress and that calculated by dividing the applied force by the undeformed cross-section is small for the first few percent of strain. In this range, constant force rate loading may be safely regarded as a constant stress rate loading. The slope of the stress-strain curve obtained by constant force rate loading is then related to the plastic strain rate for the first few percent strain by the equation

$$\frac{d\sigma}{d\epsilon_p} = \left(\frac{d\sigma}{dt} \right) \left(\frac{d\epsilon_p}{dt} \right)^{-1}$$

where σ is the applied stress, ϵ_p is the plastic strain of the specimen, and t is time.

The test was performed under a constant stress rate of 20 psi/sec. The load vs. displacement curve obtained was then transformed into engineering stress-engineering strain plot*. The stress-strain curve thus obtained is shown in Fig. 5. From this the yield stress corresponding to 0.2% strain is calculated as 4950 psi.

References:

1. N. P. Sazhin, M. G. Mil'vidskii, V. B. Osvenskii, and O. G. Stolyarov, " Influence of Doping on the Plastic Deformation of Gallium Arsenide Single Crystals ", Sov. Phys. Solid State , Vol. 8, P 1223 (1966).
2. Yasuo Tarui, Yoshio Komiya and Yasoo Harada, " Preferential Etching and Etched Profile of GaAs ", J. Electrochem. Soc., Vol. 118 [1], P 118 (1971).
3. P. L. Petrusevich and E. S. Sollertunskaya, " Detecting Dislocations on the (111) and (110) planes of Gallium Arsenide Single Crystals by the Etch Method ", Sov. Phys. Crystallography, Vol. 8, P 182 (1963).
4. E. S. Meieran. " Transmission Electron Microscope Study of Gallium Arsenide ", J. Appl. Phys., Vol. 36, P 2544 (1963).
5. D. Laister and G. M. Jenkins, " Image Contrast of Triple Loops in Tellurium-Doped Gallium Arsenide ", Phil. Mag., Vol. 20, P 361 (1971).

* The engineering stress is defined as
engineering stress = Load/ Original cross-section
and the engineering strain is defined as
engineering strain = change in length/original length.



Fig. 1a
Etch Pits on A(111) face GaAs.
Magnification 600 x

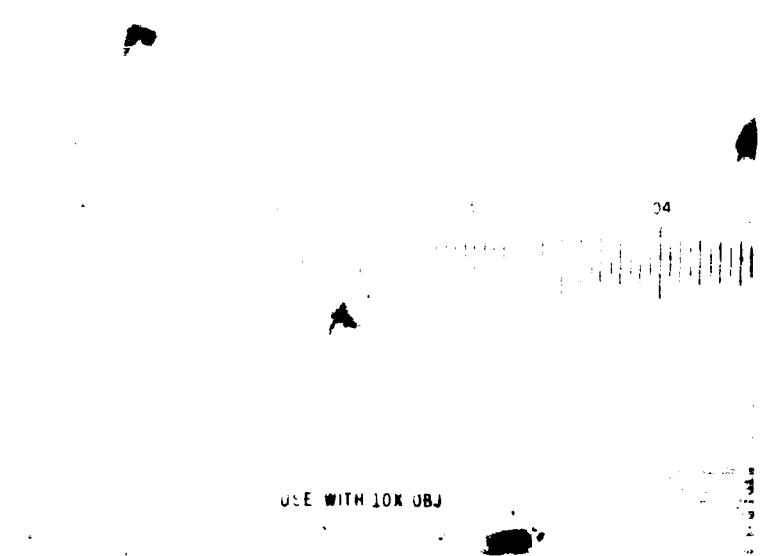
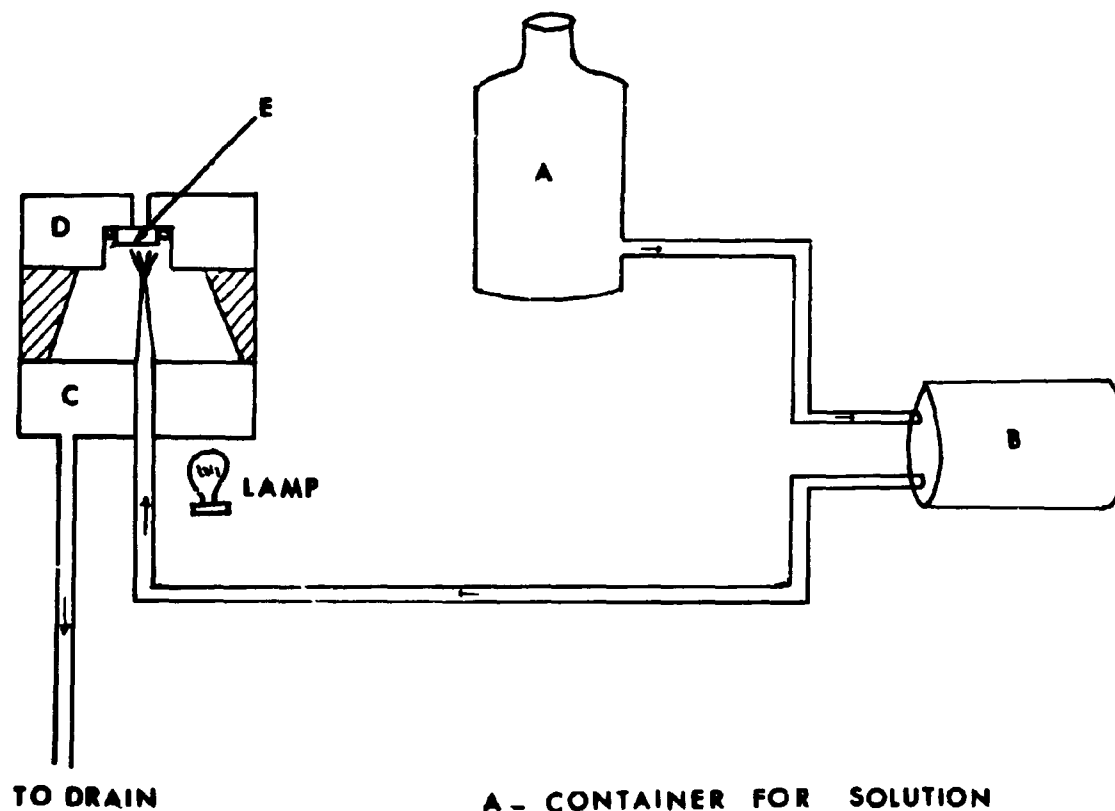


Fig. 1b
Etch Pits on an oblique face.
Magnification 300 x

△ OBSERVATION

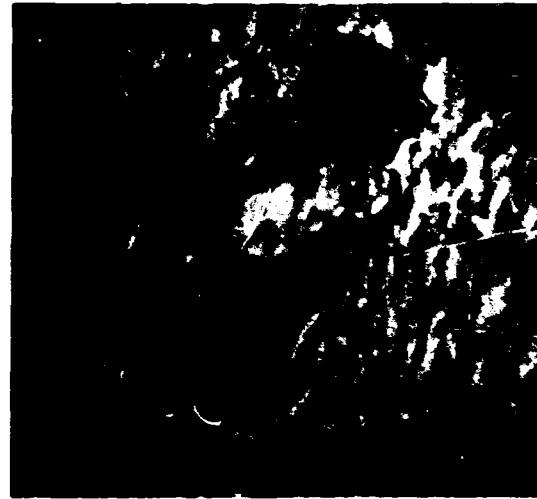


- A - CONTAINER FOR SOLUTION
- B - PUMP
- C - TEFLON CONTAINER
- D - TEFLON CONTAINER & CAP
- E - SPECIMEN BETWEEN O RINGS

Fig. 2 Schematic drawing of the Jet Polishing Equipment



a



b

Fig. 3

Typical electron micrographs of Si doped GaAs (3500x) (a) line network with what appear to be precipitates (b) bright field micrograph showing multilayer stacking faults.

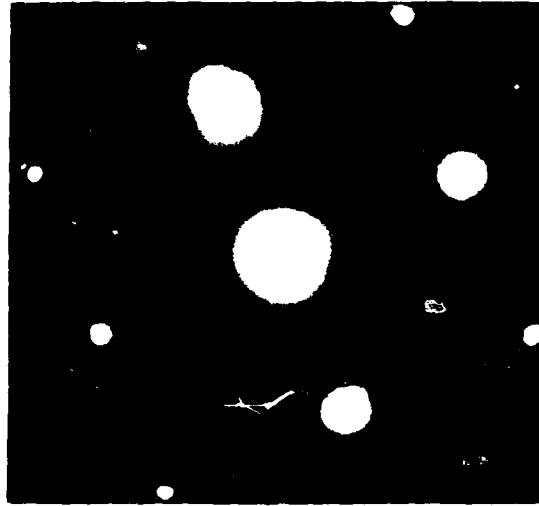


Fig. 4
A $\langle 100 \rangle$ electron diffraction pattern
from Si doped GaAs showing extra
spots and streaks.

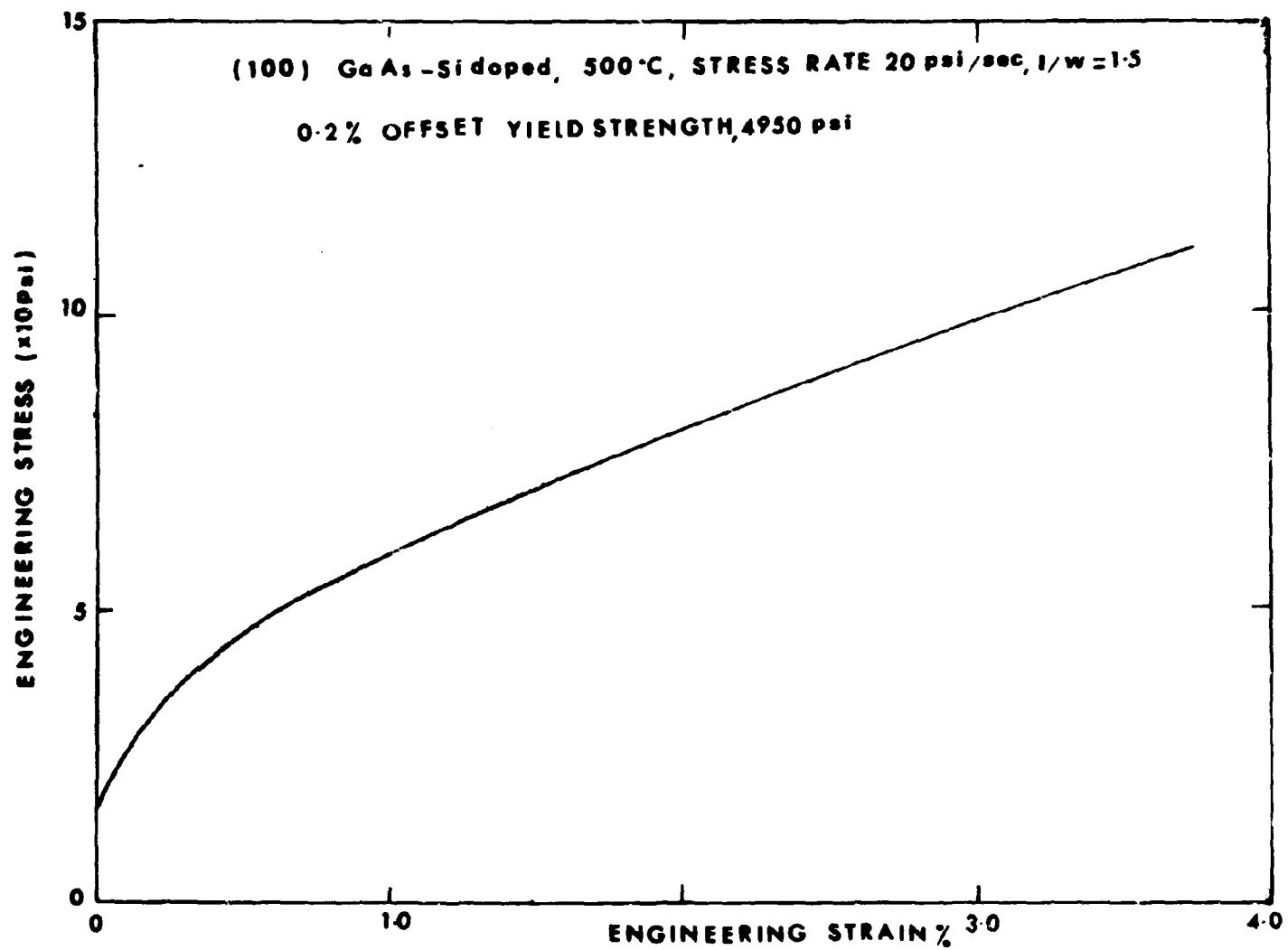


Fig. 5 Engineering Stress vs. Engineering Strain Curve for (100)
Stress axis Si doped GaAs at 500°C

d. 1. Surface and Interface IR Absorption

C. R. Crowell, T. Mangir

As one of the potential mechanisms which lead to the destruction of the optical materials we have undertaken to study the surface- and interface effects on IR absorption. Our primary objective is to establish the magnitude of these effects on GaAs surface and interfaces through the electrical measurement of surface conductivity and capacitance of the GaAs - MOS type structures.

Our first concern has been to study the air-GaAs interface with the use of an air-dielectric MOS structure. On this line, we have made studies on the preparation of GaAs surfaces.

Since sensitivity of the measurements require a small air gap, it is important that the surfaces employed in electrical testing be flat. We had decided on an air gap magnitude of $\sim 2000 \text{ \AA}$ and studied the feasibility of this order of flatness on the GaAs surfaces. We have attempted to establish the thickness of the air gap by the thickness of the evaporated metal film on the GaAs. The film is deposited in a pattern determined by a shadow mask. During device operation this film is contacted by the metallized registered pattern which is deposited on optically flat insulating substrate which is also used to support the gate electrode.

For preparation of GaAs wafers we have used mechanical-chemical polishing on some samples, which produced the required flatness over a 40 mil diameter area which is the device size intended. One disadvantage of this method is the introduction of dislocations during mechanical polishing.

Another method we used for surface preparation instead of mechanical polishing was a fast etch (HF-HNO_3) to remove the saw damaged layer on the wafers, thus avoiding the introduction of additional defects to the sample

To test the surfaces so prepared, we deposited Schottky barrier diodes and observed the I-V characteristics. Theoretically the I-V relation in Schottky diodes is:

$$I \propto e^{qV/nkT}$$

where n is typically $n \sim 1.02$ for the forward characteristic.

In our case we observed $n \approx 1.8$ for Pt-n GaAs diodes. The high value of n suggests that the present surface preparation techniques used must be improved (maybe by using longer etching times).

At present, we are measuring the capacitance of the MOS structures. Observed order of magnitude of capacitance is in agreement with the expected value.

We are also in the process of making C-V and C- ω measurements for the MOS structures, but at this time there are no definitive results available due to some technical difficulties.

During the next quarter, we will try to complete the above measurements which will then supply us with the necessary information about air GaAs interface.

d. 2. Study of Defects in II-VI Compounds

F. A. Kroger, M. Gershenson, S. S. Chern, H. R. Vydyanath

- 1) Further experiments have been carried out to clarify the abnormal, S-shaped penetration profiles of indium into CdS and CdTe.

Experiments with different diffusion times show a variation of the surface concentration for CdS but not for CdTe; this indicates the presence of a surface barrier with CdS, which might be responsible for the abnormal profile. Yet, CdTe also shows the abnormal profile but does not show signs of a surface barrier. Attempts to explain the effect by triplet formation were unsuccessful.

- 2) Te tracer self-diffusion as $f(p_{Cd})$ at 900° and $1000^{\circ}C$ show values decreasing with increasing p_{Cd} ; apparently Te_i^x is the dominant carrier in these cases.

An increase of D_{Te}^* at high p_{Cd} with p_{Cd} at $800^{\circ}C$ reported in the literature indicates Cd_i' as the dominant carrier under these conditions, Te_i^x taking over at low p_{Cd} .

- 3) Measurements of the Cd^* tracer self-diffusion of pure CdTe reported earlier were complemented with measurements on crystals doped with $\approx 2 \times 10^{17} \text{ cm}^{-3}$ indium.

The self-diffusion at low p_{Cd} is increased, that at high p_{Cd} decreased (see Fig. 1). This indicates: a) that Cd diffuses in a charged form and b) that there are two species involved: Cd_i' at high p_{Cd} and V_{Cd}'' at low p_{Cd} .

- 4) The lattice constant of CdTe, pure and doped with indium up to 10^{18} cm^{-3} was found to be $6.4820 \pm 0.001 \text{ \AA}$, independent of doping. This corresponds to a theoretical density of 5.8555 g cm^{-3} , much below the value 6.2 g cm^{-3} reported in the literature.

- 5) Experimental density determinations of CdTe ± In annealed at medium p_{Cd} show values increasing from 5.8728 to 5.8859 $g\ cm^{-3}$ with increasing indium content. This increase indicates Te_i'' rather than V_{Cd}'' as the main compensating defect in indium doped CdTe.
- 6) High-temperature Hall effect studies on "pure" CdTe as $f(p_{Cd}, T)$ show electron concentrations similar to those reported by Smith (1), at the higher temperatures, but somewhat lower at low temperatures. This indicates the presence of a foreign acceptor in our pure CdTe. In-doped crystals show increased electron concentrations (see Fig. 2). The exact In content is not known, but the data indicate concentrations of $\approx 10^{17}$ and $10^{18}\ cm^{-3}$. Analysis of the data lead to values of the equilibrium constant K''_{CdV} of the reaction:

$$Cd_{Cd}^x + 2e' \rightarrow Cd(g) + V_{Cd}''; K''_{CdV}$$

$$K''_{CdV} = \frac{p_{Cd}[V_{Cd}'']}{[e']^2} = 1.25 \times 10^{-15} \exp(-0.88\ eV/kT)\ atm\ cm^3$$

As seen in Fig. 3, the values found differ markedly from those calculated from deNobel's data (2).

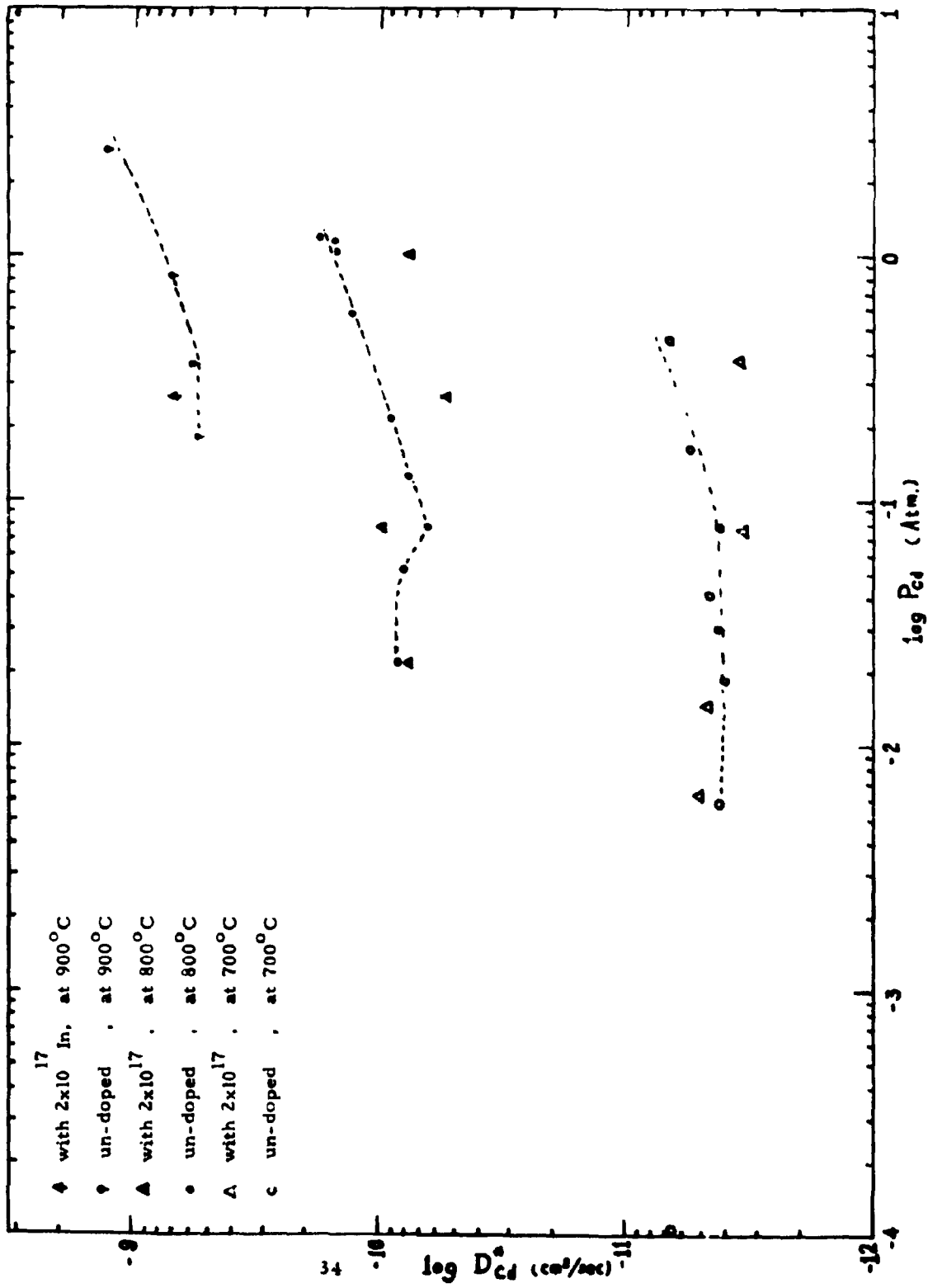
References:

- (1) F.J.J. Smith, Trans. AIME 1, 617 (1970).
- (2) D. deNobel, Philips Res. Rep. 14 (1959) 361, 430.

Intended Experiments

1. Continuation of the indium diffusion experiments.
2. Extension of the Te^* tracer diffusion at $800^\circ C$ to high p_{Cd} .
3. Extension of Cd^* tracer diffusion to more strongly doped CdTe.
4. Investigation of chemical diffusion as $f(p_{Cd}, T, [In])$.
5. Comparison of the high-temperature properties of crystals with those of cooled crystals.
6. Solubility measurements of silver in pure and donor-doped CdS at high p_{Cd} .
7. Extension of the high-temperature Hall effect studies of CdS-Ag to lower temperatures.

Fig. 1



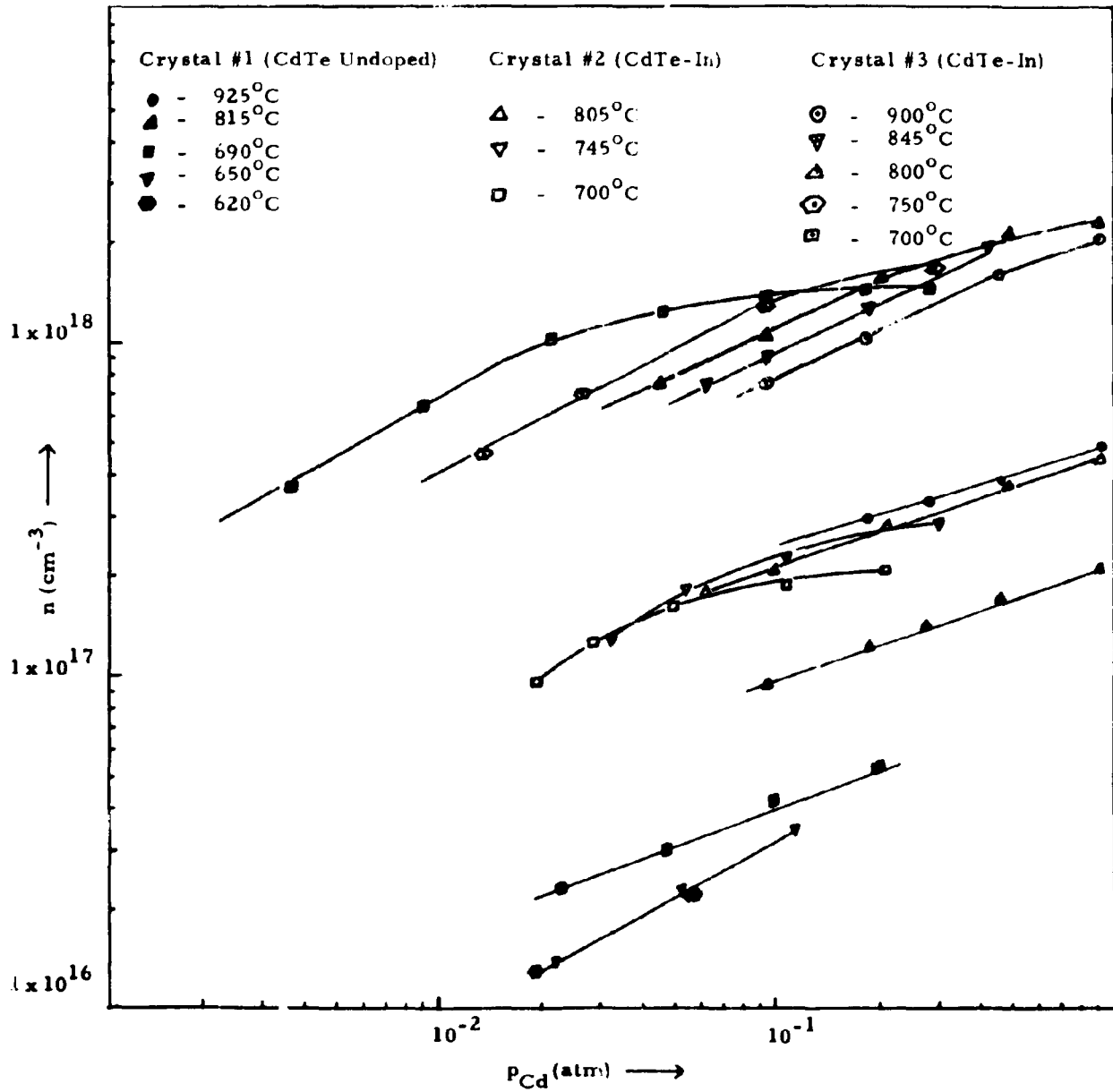


Figure 2

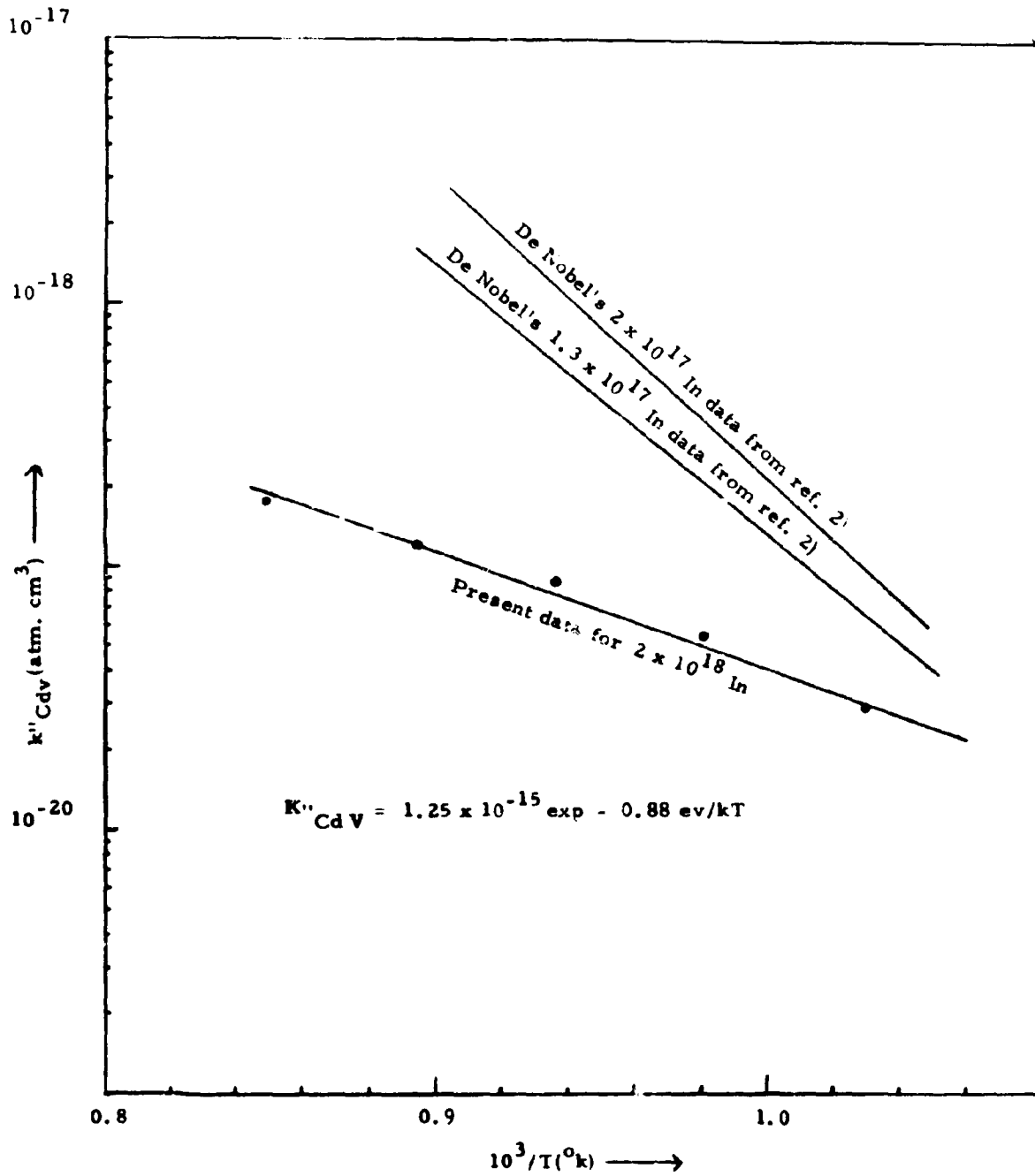


Figure 3

e. J. Theoretical Studies of Absorption Mechanisms in IR Window Materials

R. W. Hellwarth

Measurements on alkali halide (and other) crystals indicate that the absorption $\beta \text{ cm}^{-1}$ falls approximately as $\exp-A(T) \omega/\omega_0$ when the frequency ω is well above the fundamental lattice absorption frequency ω_0 . The constant $A(T)$ is typically 2 to 3 at $T = 300^\circ \text{K}$. Here we give the results of a theoretical calculation of this wing absorption by an approximation that is capable of improvement in accuracy and of extension to nonpolar crystals and crystals of different structure from the alkali halides.

This first approximation gives for the n-phonon matrix elements the same result as one would obtain for a lattice of non-interacting diatomic molecules, each bound by an effective, slightly anharmonic, potential $v(r)$. Calculating pertinent matrix elements for two trial potentials gave the following results.

1. The calculated fall-off in absorption for $\omega > \omega_0$ can be made to fit data quite well by a choice of two potential parameters that is reasonable on other grounds (comparison with dielectric and bulk modulus data). This was found to be true for both of the two forms of potential we tried, each form having repulsive core and attractive long range parts. We conclude that, at least for absorption in the range of experimental interest, our calculations are not sensitive to the choice of potential $v(r)$, and give the 'universal' approximately exponential form observed.

2. When a term quadratic in the lattice coordinate r was added to the leading linear term in the electric dipole moment, little change in the absorption tail was found (except for the highly anharmonic LiF), verifying the theoretical conclusion proposed by Keating and Rupprecht, (based on a shell model)¹ that the nonlinear part of the electric dipole moment is of minor importance to observed n-phonon absorption in alkali halides. However, the nonlinear dipole effects would be expected to dominate at absorptions many orders of magnitude lower than have been observed (except possibly for LiF where they might be affecting recent measurements.)

3. The temperature dependence we predict for the absorption at $\omega \sim n\omega_0$ is nearly of the form $(m^n - 1)/(m - 1)^n$ where $m = \exp \hbar \omega_0/kT$.

This becomes exactly true in the limit of small anharmonicity regardless of the way the electric dipole moment depends on r. Therefore there is little hope of verifying the insensitivity of the absorption to dipole nonlinearities by studying its temperature dependence. However this prediction may give a way of determining whether the absorption of a given crystal arises from the intrinsic nonlinearities discussed here, or from unwanted impurities.

4. In the limit of small anharmonicity, we find that the Morse potential spectrum (and its temperature dependence) can be written in a simple analytic form. This makes clear, for example, how the absorption depends on the nonlinear dipole term.

The real part n of the refractive index of a crystal varies little for $\omega \gg \omega_0$, and so the loss per cm β for a plane wave propagating in the crystal is given simply in terms of the net absorption rate derived from the Golden Rule:

$$\beta(\omega) = \frac{\pi \omega^3}{ncV} \sum_{m,n} (W_m - W_n) |\langle m | \sum_{\text{unit cells } \alpha} M_{\alpha} | n \rangle|^2 \delta(\omega - \omega_{nm}). \quad (1)$$

Here, M_{α} is the electric dipole moment operator for the ions in unit cell α . (Since we consider optically isotropic crystals, it does not matter which spatial component we take M_{α} to be.) The refractive index at ω is n , and $c = 3 \times 10^{10}$ cm sec⁻¹. The states $|m\rangle$ are states of a macroscopic volume V of the crystal with thermal probabilities W_m of occupation.

Using the exact expression (1), we have proceeded to calculate the wing absorption of an alkali halide crystal via the following approximations:

Approx. I. The exact expression (1) involves a double summation ($\sum_{\alpha} \sum_{\beta}$) over all unit cells. We have so far studied only the $\alpha = \beta$ terms and discuss only these terms below. Whether or not the $\alpha \neq \beta$ terms can be neglected will be studied during the next quarter. If they cannot be neglected, we will estimate their magnitudes.

Approx. II. We assume that only the optical phonons (not acoustic) are partaking in n-phonon absorption, and assume further that the optical branch dispersion is very small. That is, we assume an "Einstein" lattice whose optical branch frequencies $\omega(k)$ are a constant ω_0 which we take to be the observed fundamental lattice absorption frequency. This is equivalent to assuming that the optical branch motions

in one unit cell are independent of motions in other cells, and that these motions may be described by a simple potential function $v(r)$ of the distance r between the two ions in the unit cell. The next corrections to this approximation will also be calculated during the next quarter.

With these assumptions, we will of course obtain an absorption spectrum consisting of discrete lines corresponding to transitions between states of the diatomic molecule in the unit cell. In the real lattice the transitions form a continuum. We feel that the trend of this continuum absorption is predicted at least qualitatively by the trend of the discrete "n-phonon" lines which fall at $\omega = n\omega_0$.

The proper type of effective potential $v(r)$ to consider must obviously be nearly $(n+\frac{1}{2})\hbar\omega_0$. The small anharmonicity will cause the usual harmonic oscillator dipole selection rules to break down, and matrix elements of the form $\langle n' | (r-r_e)^m | n \rangle$ will exist between all states n, n' and for all powers m of the displacement $r-r_e$ about the equilibrium separation r_e . To use (1) for the absorption, it remains then only to find the appropriate matrix elements for the slightly anharmonic potential under consideration.

We have studied two different, slightly anharmonic, potentials; first the Morse potential:

$$v(r)/\hbar\omega_0 = \frac{1}{2}b^{-2}(e^{-2bu} - 2e^{-bu}), \quad (2)$$

and secondly the potential used by Kittel² to fit the bulk moduli of alkali halides:

$$v(r)/\hbar\omega_0 = \frac{1}{2b^2} \left[e^{-bu} - \frac{C}{1+u/u_0} \right] \quad (3)$$

Here u is the dimensionless displacement $(r-r_e)/r_0$ from equilibrium r_e in units of $r_0 = (\hbar/\mu\omega_0)^{\frac{1}{2}}$ where μ is the reduced mass. The constants C and u_0 are arranged so that the RHS has the form $\frac{1}{2}u^2[1+C_1bu + C_2(bu)^2 + \dots]$.

The results of using either potential are practically the same. The spectra for the second potential (3) have been calculated both by numerical and perturbation methods in collaboration with T. C. McGill.³ These spectra have almost identical shapes, in the absorption regions of interest, to those of the Morse potential. We will concentrate here on the Morse potential results for which more analytical approximations exist; the other results will be presented elsewhere.³

For the electric dipole moment operator, we have used the form

$$M = e^* r_0 \left[u + S \left(r_e / r_0 \right) u^2 \right] \quad (4)$$

where e^* is the effective charge. The dimensionless parameter S has been traditionally used to measure the deviation of the moment from linearity in fitting diatomic molecule vapor spectra.^{4, 5}

Morse potential states have energies

$$E_n = \hbar \omega_0 \left[n + \frac{1}{2} + x \left(n + \frac{1}{2} \right)^2 \right]; \quad x \equiv \frac{1}{2} b^2 \quad (5)$$

The linear dipole matrix elements are

$$u_{mn} = (-1)^{m+n+1} \left\{ \frac{[1-(2m+1)x]}{[1-(m+1)x]} \frac{[1-(2n+1)x] x^{n-m-1} n!}{[1-(m+2)x] \cdots [1-nx] m!} \right\} \quad (6)$$

for $n > m$. The complicated formula for the matrix elements $(u^2)_{mn}$ of the quadratic part of the dipole operator M between Morse-potential state has been written previously, and we will not repeat it here.⁽⁴⁾ We have used these known matrix elements of (4) in (1) to calculate the absorption of various Morse potentials whose parameters e^* and x have been adjusted by eye (with $\omega_0 = \omega_{TO}$) to give a good fit to the experimentally observed absorption tails in KBr, KCl, NaCl, and LiF at 300° K. The fitting was performed first with no nonlinear moment term ($S=0$) and then the spectra were recomputed with the same e^* and x but with the temperature changed to 0° K. The results are plotted on Figs. 1a-d along with the recently measured absorption tails.⁽⁶⁾ Each of the theoretical points at the frequency $n\omega_0$ represents the thermally weighted sum of the absorption strengths of all (up and down) n -step transitions in (1), normalized to fit the measured absorption tail. Of course, the levels of the Morse potential deviate (by 5) from equal spacing, but we ignore this in these qualitative comparisons. We feel the molecular model is more useful for estimating the n -phonon matrix elements than for dealing with the phonon energy dispersion.

We have repeated our Morse-potential absorption calculations at 300° K using the same parameters as above but adding the contribution from the quadratic term in the dipole moment. The vapor spectra of OH,

CO, HCl and other molecules have been fitted with a Morse potential and values of the nonlinear moment parameter S ranging from 0.1 to 0.3. (5) To obtain a qualitative idea of the effect of S in the crystals, we have calculated the absorption with our model for $S=0.1, 0.3,$ and 0.5 . We obtained corrections to Figs. 1a-c which would barely be seen on these plots, except for LiF whose large anharmonicity x makes them prominent. The corrections to the calculated KBr absorption are given in Fig. 2.

Finally, we note that if one assumes a linear dipole moment ($S=0$) and small anharmonicity ($x \ll 1$) i. e., so that the probability of being in state m is proportional to $\exp(-m\hbar \omega_0/kT)$, and then keeps only the lowest order terms in the anharmonicity parameter x of the matrix elements (6), then the expression (1) for the absorption β_n at frequency $n\omega_0$ is easily verified to sum to

$$\beta_n/\beta_1 = 2nc_n^2 n! (e^{yn} - 1)/(e^y - 1)^n, \quad n^2 x \ll 1, \quad (7)$$

$$\text{where } y \equiv \hbar \omega_0/kT \text{ and } c_n \equiv 2^{-n/2} n^{-1} (-b)^{n-1} \quad (8)$$

When $S \neq 0$, the existence of the quadratic part of the moment alters the expression (B5) as follows. Substitute in (B5), instead of c_n , the altered coefficients \bar{c}_n defined by

$$\bar{c}_n = c_n + S(r_0/r_e) \left[2^{1-n/2} \left(\frac{1}{1(n-1)} + \frac{1}{2(n-2)} + \dots + \frac{1}{(n/2)^2} \right) \right]^{-n-2} 2^{2-n/2} b^{n-2}, \quad (9)$$

for n even and

$$\bar{c}_n = c_n - S(r_0/r_e) 2^{1-n/2} \left[\frac{1}{n-1} + \frac{1}{2(n-2)} + \frac{1}{3(n-3)} + \dots + \frac{1}{\frac{n+1}{2}} \frac{1}{\frac{n-1}{2}} \right] b^{n-2} \quad (10)$$

for n odd and > 2 . (Note that the series in (9) and (10) terminate with the first term for $n=2$ and 3 , respectively.) It is seen that normally ($S > 0$) the terms from the $(u^2)_{mn}$ matrix elements tend to cancel those from u_{mn} , and that as ω/ω_0 gets larger, the $(u^2)_{mn}$ parts gradually begin to dominate, making the absorption fall off much less slowly at high ω than if $S=0$. It is also seen from inspection of (7)-(10) that the presence of a significant nonlinear moment should not greatly alter the temperature dependence of the absorption nor change its dependence on the anharmonicity parameter $x=b^2/2$.

We have verified that the parameters ϵ^* and b which we need to fit the absorption tails are of the same order of magnitude as the values we would need to fit the dielectric constant and the bulk modulus with crude theory employing the same forms (2) and (3).

We plan to estimate the nature of the errors inherent in the first approximation to the tail absorption for alkali halides discussed above. However, prime emphasis will be on extending the theory to treat more complicated crystals, especially GaAs, CdTe, and Ge.

References

1. P. N. Keating and G. Rupprecht, Phys. Rev. 138A, 866 (1965).
2. C. Kittel, Introduction to Solid State Physics, 4th Ed., Chapter 3 (John Wiley, New York 1971).
3. T. C. McGill, R. W. Hellwarth and M. Mangir, "Infrared Absorption in Insulators due to Multiphonon Processes" (to be published).
4. H. S. Heaks and G. Herzberg, Zeit, fur Physik 133, 48 (1952).
5. R. A. Toth, R. H. Hunt, and E. K. Pyle., J. Mol. Spect. 35, 110 (1970); 32, 85 (1969); and 32, 74 (1969). These authors give many other references to work to determine the nonlinear dipole moment functions of molecules.
6. T. F. Deutsch (to be published).

Figure Captions for Appendix Figures

Fig. 1 measured absorption wing (solid line) and calculated n-phonon absorption from Morse potential at 300° K (indicated by crosses +) and at 0° K (Indicated by squares ■) for a) KBr, b) KCl, c) NaCl, and d) LiF. In 1-d the absorption at 300° K, as altered by adding a quadratic component of $S = 0.3$ to the dipole moment of (B2), is indicated by circles (O). In each case the anharmonicity parameter x and equilibrium distance parameter r_0/r_e assumed is stated in the figure.

Fig. 2 the changes in the average n-phonon absorption strength ($n=\omega/\omega_0$) at 300° K caused by addition of quadratic components of dipole moment of $S=0.3$ and 0.5 to the Morse potential calculation for KBr.

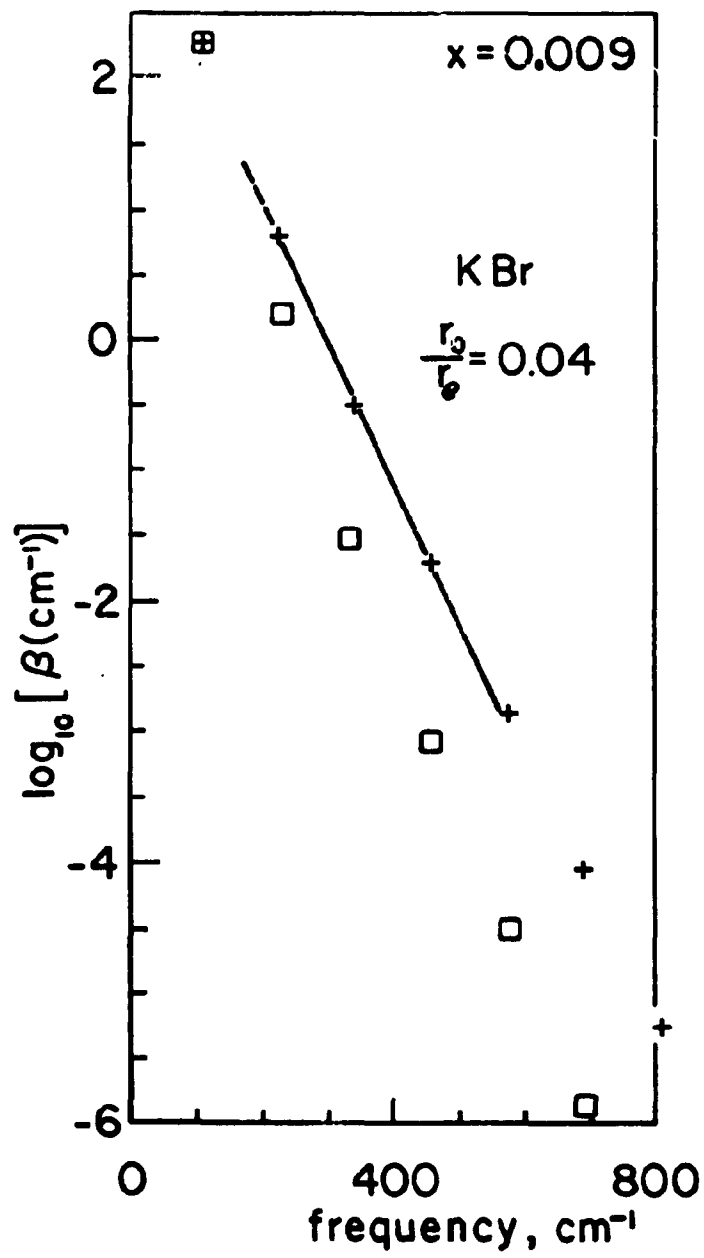


Fig. 1a

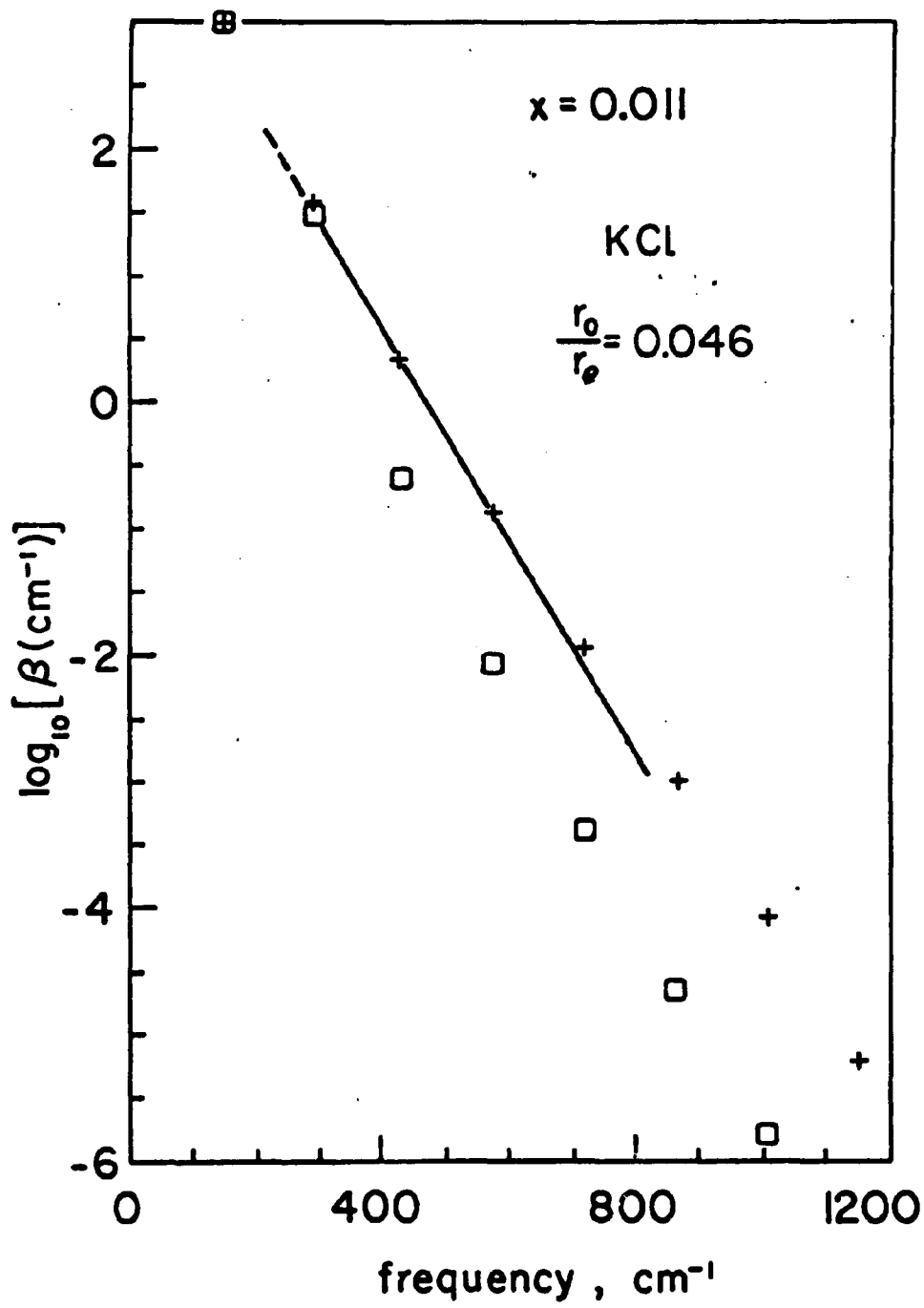


Fig. 1b
46

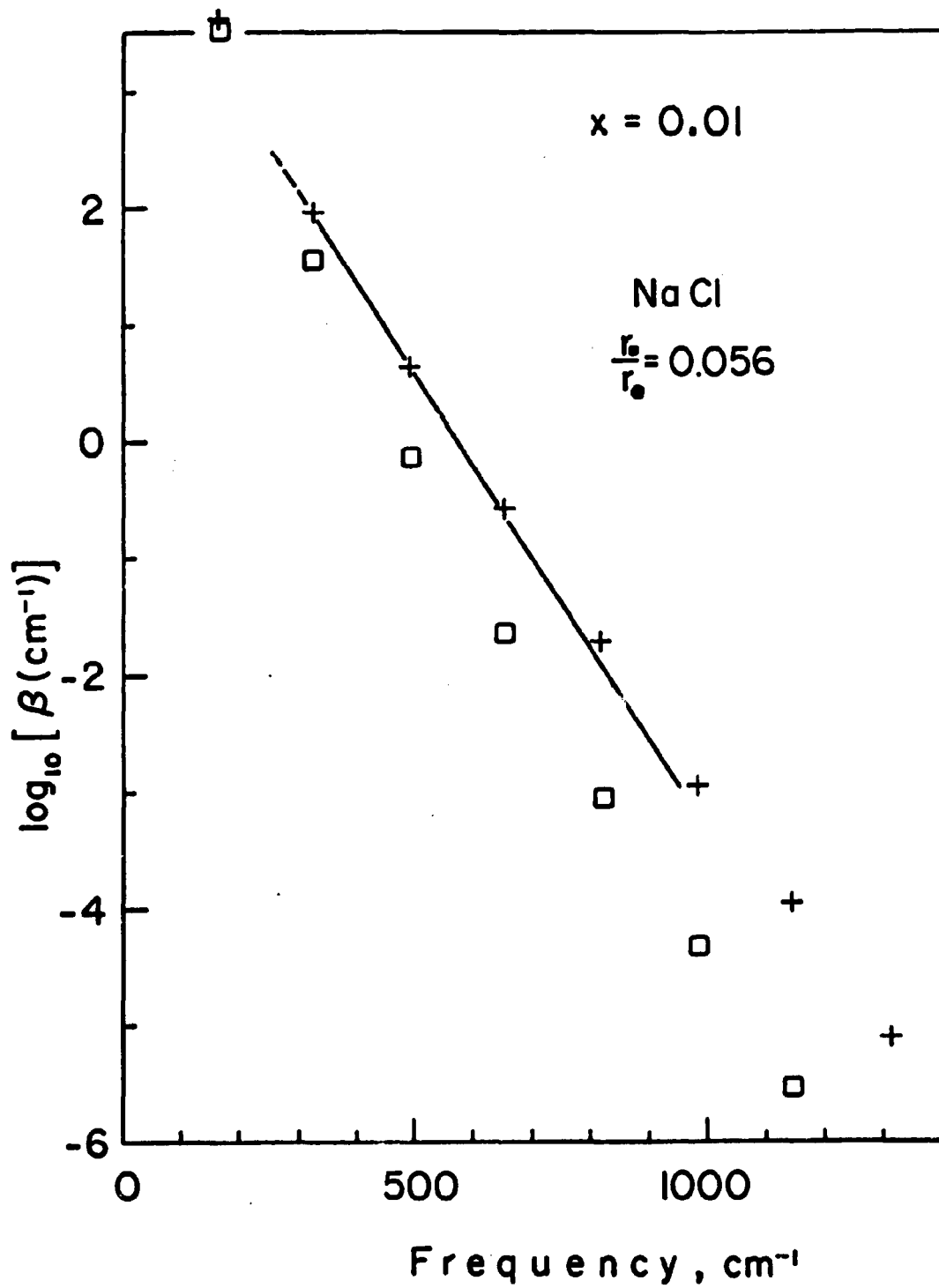
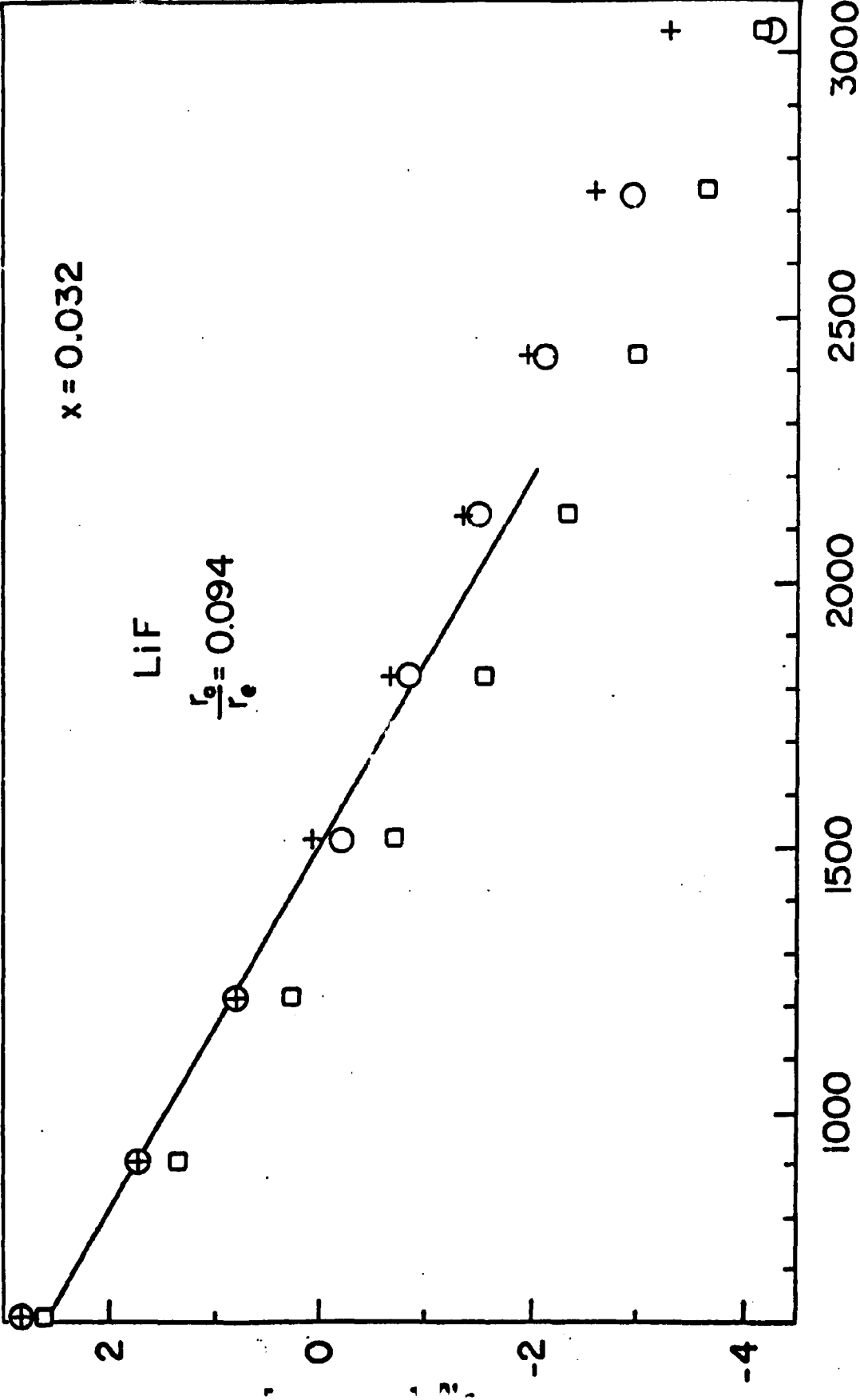


Fig. 1c
47



Frequency, cm⁻¹
 Fig. 1d

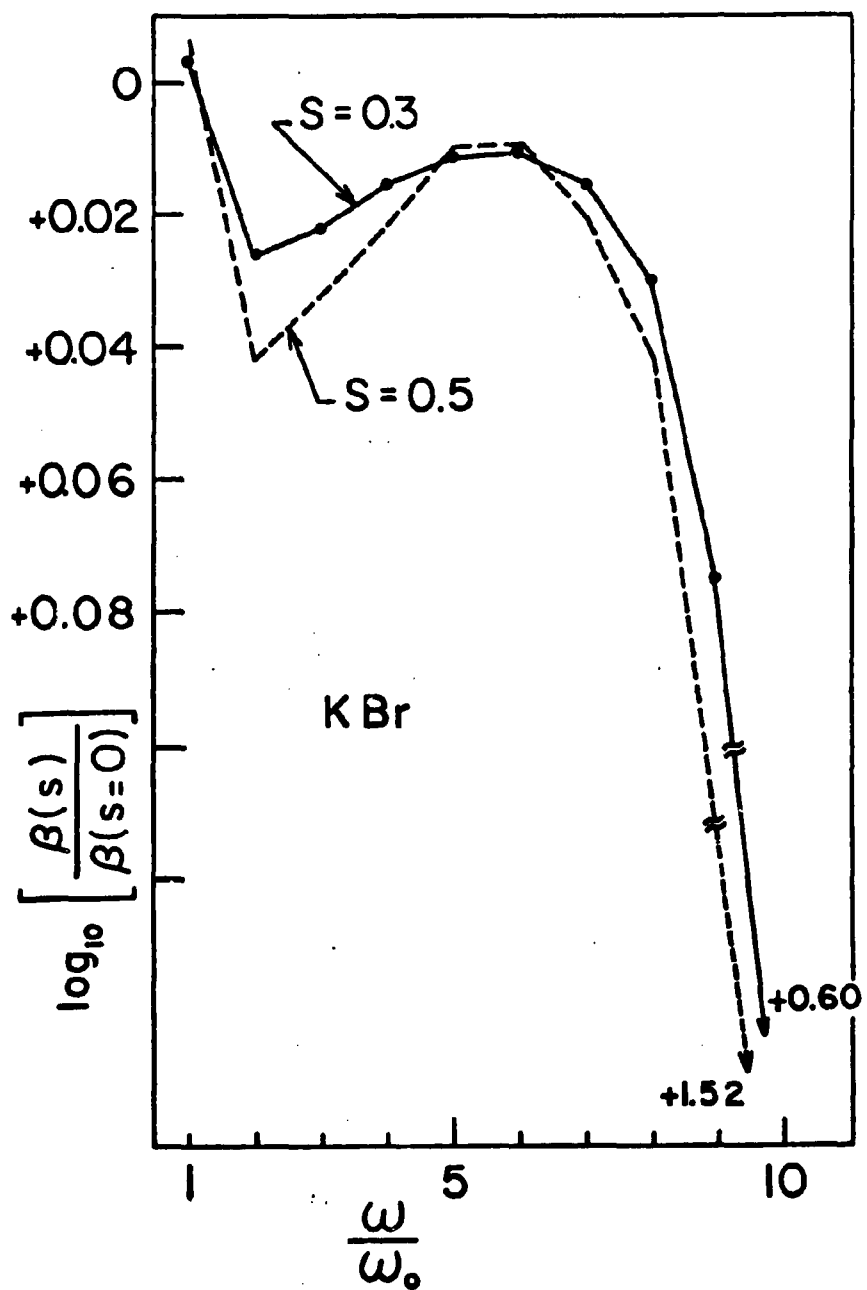


Fig. 2
49

f.1 Techniques for Indirect Measurement of Small Absorptive Losses

W. H. Steier, S. T. K. Nieh

Calorimetric Loss Measurements

A. Check Against Known Sample

The calorimeter for measuring absorption coefficients at wavelengths around 10μ is completed and in use. With the experience obtained in the last quarter we are fairly confident of the measurements and able to recognize errors when they appear. The absorption coefficient of samples obtained from AFCRL have been measured and our results agree with the previously measured values.

From the measured heating curves we can readily determine if direct illumination of the thermocouples has occurred and if the thermal bond between the sample and thermocouple is good. The TC is placed in a small drilled hole in the sample and attached with heat sink compound. The sample is held by a three point low thermal conductance jig and shielded from room air currents. The transmitted 10μ power is measured by a Model 201 CRL power meter whose calibration has been crosschecked against a Scientech Md 3610 power meter.

Table I shows our measured absorption coefficient of a GaAs sample obtained from AFCRL. The average of these measurements is 0.040 cm^{-1} which is in agreement with the AFCRL measurements of 0.04 cm^{-1} . These results indicate that the calorimeter is accurate for measurements in the range of $.04 \text{ cm}^{-1}$ and we believe our current setup is accurate down to 0.001 cm^{-1} . For measurements of α less than 0.001 cm^{-1} evacuation of the chamber around the sample will probably be necessary. Room air currents appear to be largest contributor to instabilities and TC drift.

B. Measurements on High-Resistivity Un-Doped GaAs

High-purity un-doped GaAs, grown at USC, has been measured and appears to be among the lowest loss GaAs yet reported. The crystal group at USC has had considerable experience in high purity GaAs crystal growth under previous contract support and techniques have

been developed for the growth of high purity, high resistivity material which is un-doped. Material grown by the horizontal Bridgeman technique has resulted in un-doped material with $10^8 \Omega\text{-cm}$ resistivity. The 10μ absorption coefficient of a sample of this material, taken from a boule denoted by WA 1000, has been measured and the results are shown in Table II.

The loss coefficient of 0.005 cm^{-1} measured at 9.28μ is the lowest yet reported for GaAs using the CO_2 laser lines. Previously reported measurements on GaAs have been made at 10.6μ where the lowest reported number is 0.006 cm^{-1} . Our measurements near 10.6μ (10.48μ) give an α of 0.008 cm^{-1} .

We have observed a repeatable structure in the measurement of α vs. λ over the range from 9.2 to 10.6μ . Over this band the loss coefficient varies by a factor of 2 (see Table II). To our knowledge this is the first calorimetric measurement of α vs. λ and we hope this data will shed some light on the source of the loss. Repeated measurements at a fixed λ (see Table II) show that the variation of α with λ is not due to inaccuracies in our measurement. Preliminary measurements at wavelengths near those given in Table II indicate a smooth variation of α with λ and confirm the structure.

This measurement is possible because our relatively large laser ($\sim 3\text{m}$ long) has sufficient power output over a wide band when a grating wavelength selector is used in the cavity. We are currently repolishing and reshaping this sample to a more nearly circular cross-section and we plan to do a complete measurement of α vs. λ over the range of λ possible with our laser.

The transmitted power through this sample varies considerably with the tilt of the sample relative to the beam; indicating a strong Fabry-Perot effect as expected of a low loss sample. We normally set the sample angle for maximum transmission which is near 80%. However, we have verified that the measured α is independent of the sample angle.

We are obtaining samples of hi-resistivity un-doped and hi-resistivity compensated GaAs from several sources and plan to measure α vs. λ

for those samples which are low loss. We are also in the process of obtaining another boule of undoped GaAs grown by the same techniques as WA-1000.

TABLE I

GaAs-AFCRL #G-4-17-2

8mm X 16 mm X 1.8 mm

wt. -0.82 gm

AFCRL measured $\alpha = 0.04\text{cm}^{-1}$

Run #	Transmitted Power (W)	α (cm^{-1})
1	0.85	0.038
2	0.66	0.039
3	1.16	0.041
4*	1.22	0.040
5*	2.2	0.0415
6*	2.5	0.0385

*Sample and thermocouple were remounted after run #3

TABLE II

Hi-Resistivity Undoped GaAs - Horizontal Bridgeman (WA-1000)

$$\rho = 10^8 \text{ ohm-cm} \quad \mu = 2000 \frac{\text{cm}^2}{\text{volt-sec}}$$

Run#	Wavelength (μ)	P_{tr} (Watt)	α (cm^{-1})
10	9.28	3.2	0.0051
11	9.28	1.81	0.0050
12	9.28	3.04	0.0054
13	9.57	3.7	0.0105
14	9.57	1.36	0.0113
15	9.57	2.26	0.0101
20	10.48	1.32	0.0081
21	10.48	2.5	0.0081

Sample dimensions-27mm x 13mm (irregular) x 2.08mm
wt. -3.1 gm

g.1 Characterization of Optical Performance of IR Window Systems

M. Flannery, J. H. Marburger

(1) INTRODUCTION

In our previous report, we described a two-dimensional computer code for determining the influence of a thin thermally distorted window on the optical field of a coherent beam focused through it. One of the phenomena which can be analyzed with such a code is the skewing or slewing of an asymmetric beam due to the "thermal prism" which it induces in the window. Computer generated plots of this phenomenon were reported in the previous report. While that work was being prepared for the report, Dr. L. Skolnik at AFCRL observed a slewing effect experimentally. During this period, we have attempted to reproduce the observed slew magnitude theoretically. This would be an important check on the magnitude of parameters, such as absorption coefficient and rate of change of refractive index with temperature, which contribute to the effect.

Since we do not have a code which determines the temperature distribution in a window heated asymmetrically, we decided to approximate the effect in one dimension with "slab shaped" unsymmetric beams. The resulting one dimensional heat flow problem is easily solved numerically and in some cases analytically, and is discussed in Section 2 below. Using computer codes discussed in Section 3, we simulated the experiment of Skolnik.

In Skolnik's experiment, a KCl window (5cm diam. x 0.3cm thick) was illuminated by a 95 watt "Gaussian" CO₂ laser beam with $1/e^2$ intensity diameter 1.05 cm at the window. Beam scans taken at 42 watts showed a slight asymmetry of the incident beam, and to this was attributed the observed slew of 10^{-3} (4 mm in 4 meters. We define the slew as the tangent of the slew angle, which in most cases equals the angle itself). For more details of this experiment, see ref. 1.

Using material parameters for KCl compiled by Sparks² and beam parameters communicated by Skolnik, we found an unobservably small slew, as indicated in Fig. 3 below. Increasing asymmetry and absorption

coefficient by orders of magnitude did not lead to slews comparable with those observed by Skolnik.

The significance of this negative result must be assessed in the light of approximations which we made in the numerical simulation. The most severe assumption is that the slew of a three-dimensional beam can be inferred from that of a two-dimensional "slab-shaped" beam. We believe that the slewing effect will be magnified in the lower dimensionality because 1) The effect of thermal conduction is to weaken the induced thermal prism in the direction perpendicular to the line L along which the greatest asymmetry is measured. In a slab-shaped beam, there is no heat flow along this direction, which is taken to be the direction along the slab. 2) Rays which do not pass through the Line L are not deflected as much as rays on the line. Thus the maximum deflection occurs only for a small percentage of the rays passing through the window. In a slab shaped beam, all the rays experience the maximum deflection.

The second important feature omitted from the simulation is the effect of thermally induced birefringence. We believe that this effect is important, but comparable to the isotropic effects which were included in the code. It is difficult to see how omission of this effect could cause the results to be off by orders of magnitude, (which is the size of the discrepancy between theory and experiment.) Therefore, we conclude that the slewing observed by Skolnik cannot be understood in terms of the reported values of the material parameters for KCl and the reported beam parameters.

(2) ANALYSIS OF ONE DIMENSIONAL WINDOW PROBLEM

We assume the intensity distribution in the beam at the window is independent of the coordinate η and is asymmetric along the orthogonal coordinate ξ (see Fig. 1). The transmitted intensity at point x, y, z and time τ is the one dimensional form of equation (1) in the previous report (the Huygens-Fresnel integral). The amplitude in the aperture, which enters this equation, was taken to be

$$A(\xi', \tau) = \sqrt{I_0} a(\xi') \exp i k' P(\xi', \tau) \quad (1)$$

where primed quantities are dimensionless coordinates $x' = x/D$ etc., and D is the half the window width. τ is a dimensionless time defined below.

The change in optical path length of the beam in the window is related to the temperature through the formula

$$P(\xi, t) = L \left[(n-1) \alpha_L + \frac{\partial n}{\partial T} \right] T(\xi, t) \quad (2)$$

where L is the window thickness. T is the temperature distribution which satisfies the heat equation

$$\frac{\partial T}{\partial t} = \kappa \frac{\partial^2 T}{\partial \xi^2} + \frac{\beta I_0}{C} \phi(\xi), \quad \phi(\xi) = |a(\xi)|^2. \quad (3)$$

This can be rewritten as an equation for $P' = P/D$,

$$\frac{\partial P'}{\partial \tau} = \frac{\partial^2 P'}{\partial \xi'^2} + G \phi(\xi') \quad (4)$$

Where $\tau = \kappa t / D^2$,

$$G = \frac{\beta I_0 L D}{\kappa C} \left[(n-1) \alpha_L + \frac{\partial n}{\partial T} \right]. \quad (5)$$

Notice that all material parameters are contained in G and the dimensionless time.

Analytical solutions of (4) were obtained in the special case where

$$\phi(\xi') = \alpha + \beta \xi' + \gamma \xi'^2 + \delta \xi'^3 \quad (6)$$

and for boundary conditions corresponding to edge cooling and conduction to infinity (infinitely large window). The solutions obtained were cumbersome and will not be reported here. They are useful for checking numerical solutions, but the form (6) is too restrictive for our purposes.

(3) NUMERICAL SIMULATION OF BEAM SLEWING

The one dimensional heat equation (4) was solved numerically using the Crank-Nicolson method. The window edges are at E_1 and E_2 as shown in Fig. 1 and the window aperture, where the light is admitted, is the opening $(-D, D)$. The portion of the window beyond the aperture allows different thermal boundary conditions to be simulated. The edges E_1, E_2 can be moved about to simulate off-center beams.

The beam profile employed was gaussian with an asymmetry correction

$$\phi(\xi) = \exp(-W\xi^2) + \Psi(\xi)$$

where $W = 7.256$, and Ψ was provided by L. Skolnik. The asymmetry correction actually used is plotted in Fig. 2. The aperture was placed at the $\exp(-4.5)$ point of the gaussian: $D = 0.7875$.

Using data on KCl compiled by Sparks², and the values $L = 0.3$ cm, window width $2D = 1.58$ cm, maximum on axis intensity $I_0 = 300$ W/cm², distance to observation point = 4 m, we find

$$G_0 = -0.86 \times 10^{-5}.$$

The window edges were placed at ± 2.5 cm and the beam was focused at "infinity" (10^6 meters).

A selection of the computer simulations are shown in Figs. 3-6. The curves are labelled with the parameter τ , where $\tau=1$ is equivalent to 12.85 seconds. The x' axis is in units of D , so $x' = 1.27$ corresponds to a distance of 1 cm.

Figure 3 which shows hardly any distortion at all, is the simulation for $G=G_0$. This run uses without modification the parameters supplied by L. Skolnik. There is essentially no slewing effect at all. The subsequent figures represent our attempts to reproduce the experimental slew by changing various parameters. Thus in Fig. 4, G was multiplied by 100 to simulate a large absorption and the asymmetry function was doubled. In Fig. 5 G was multiplied by 1000. Figure 6 corresponds to a grossly uncentered beam, where $E_1 = D, E_2 = 2.5$ cm and $G = 150 G_0$. This caused more slewing than any of the other cases and the steady state beam shape resembles the experimental shape.

(4) DISCUSSION

Unless there is another mechanism for beam slewing inherent in Skolnik's experimental procedure, our theoretical results indicate that the material parameters and the reported experimental results are inconsistent. During the next meeting period, we shall attempt to discover the source of this discrepancy.

REFERENCES

- 1) L. Skolnik, Second Conference on High Power Infrared Laser Window Materials, 31 Oct. and 1 Nov., 1972, Hyannis, Mass. (to be published)
- 2) M. Sparks, "Optical Distortion by Heated Windows in High-Power Laser Systems" Preprint, Feb. 1971.

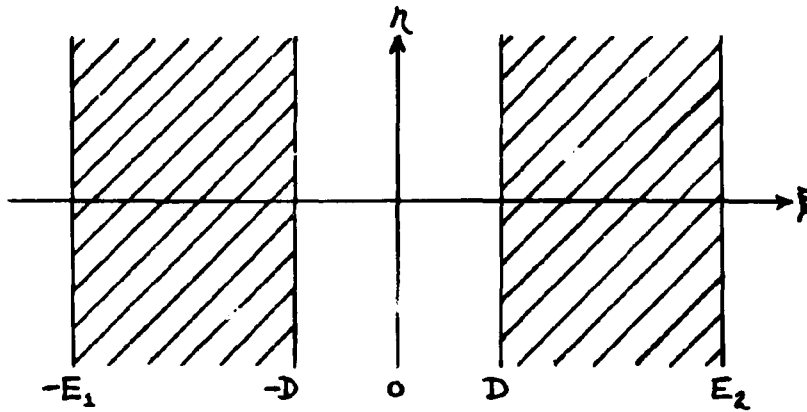


Fig. 1

The Aperture and Window extend to Infinity in the η -direction, with edges at $(-D, D)$ and $(-E_1, E_2)$ respectively.

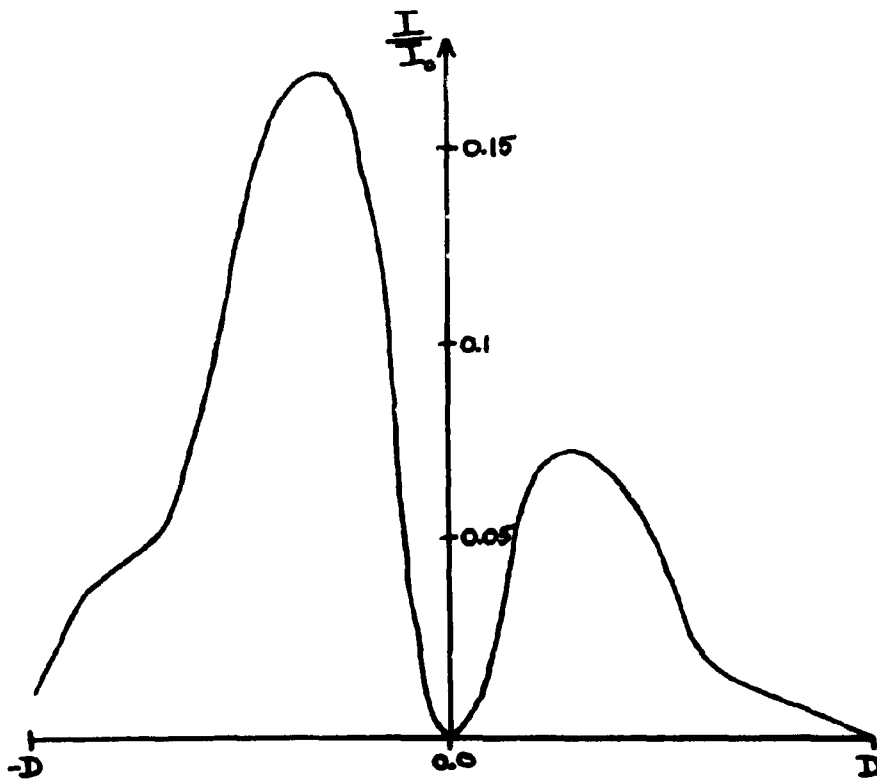


Fig. 2

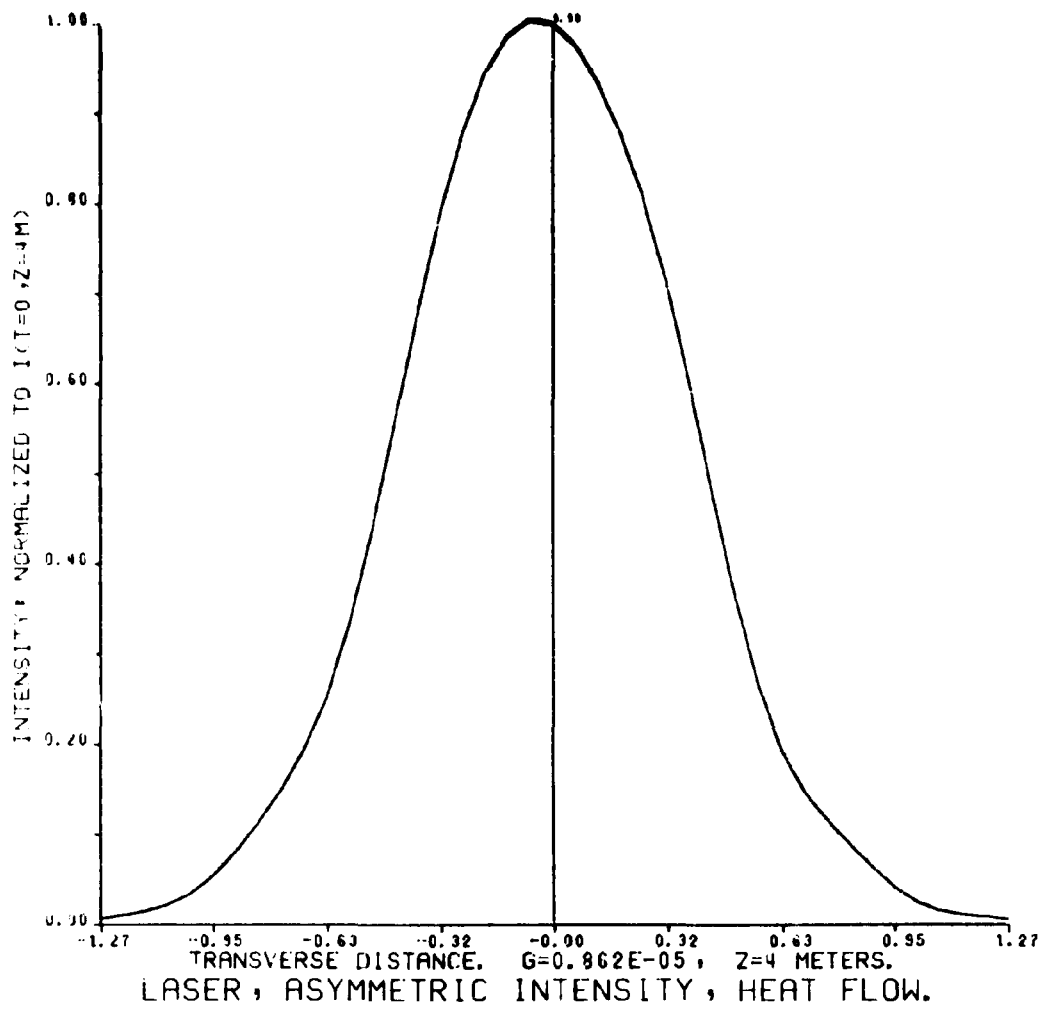


Fig. 3

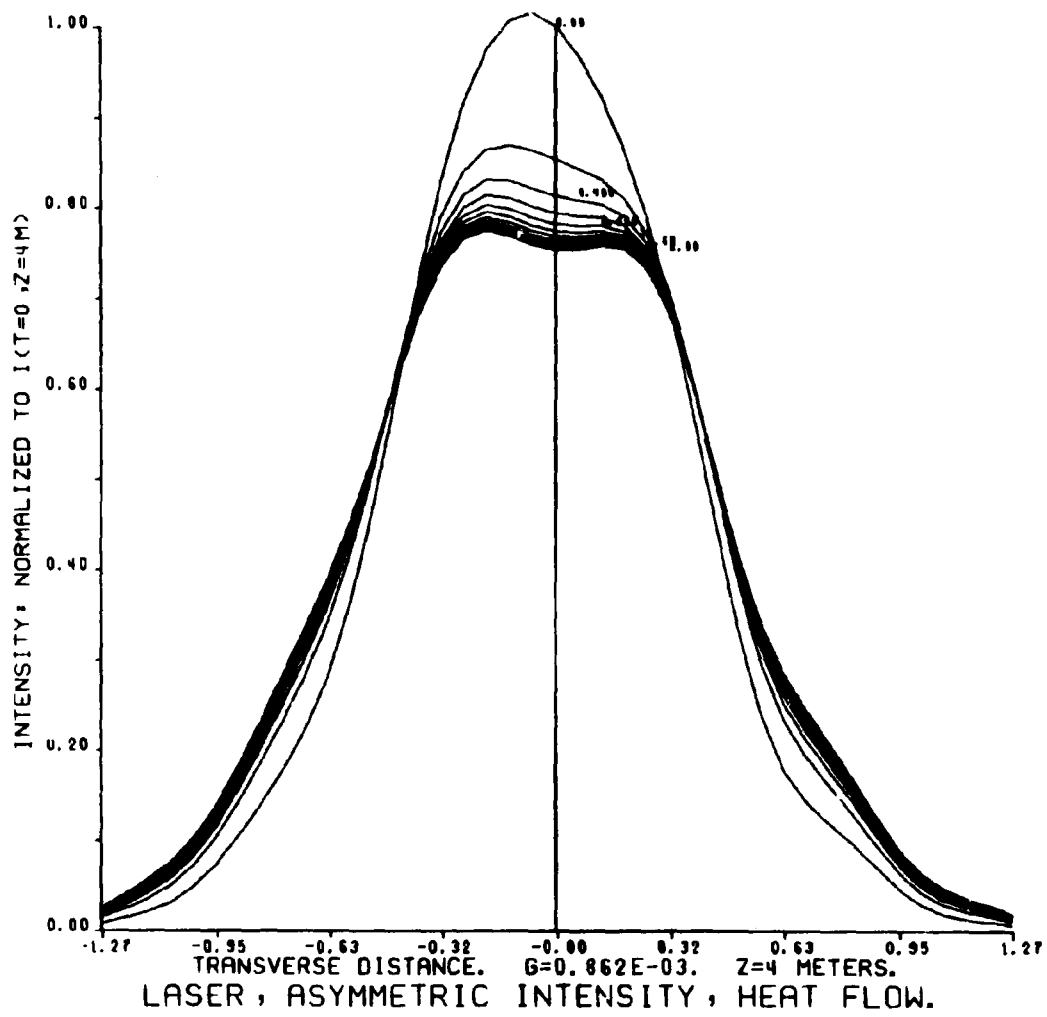


Fig. 4

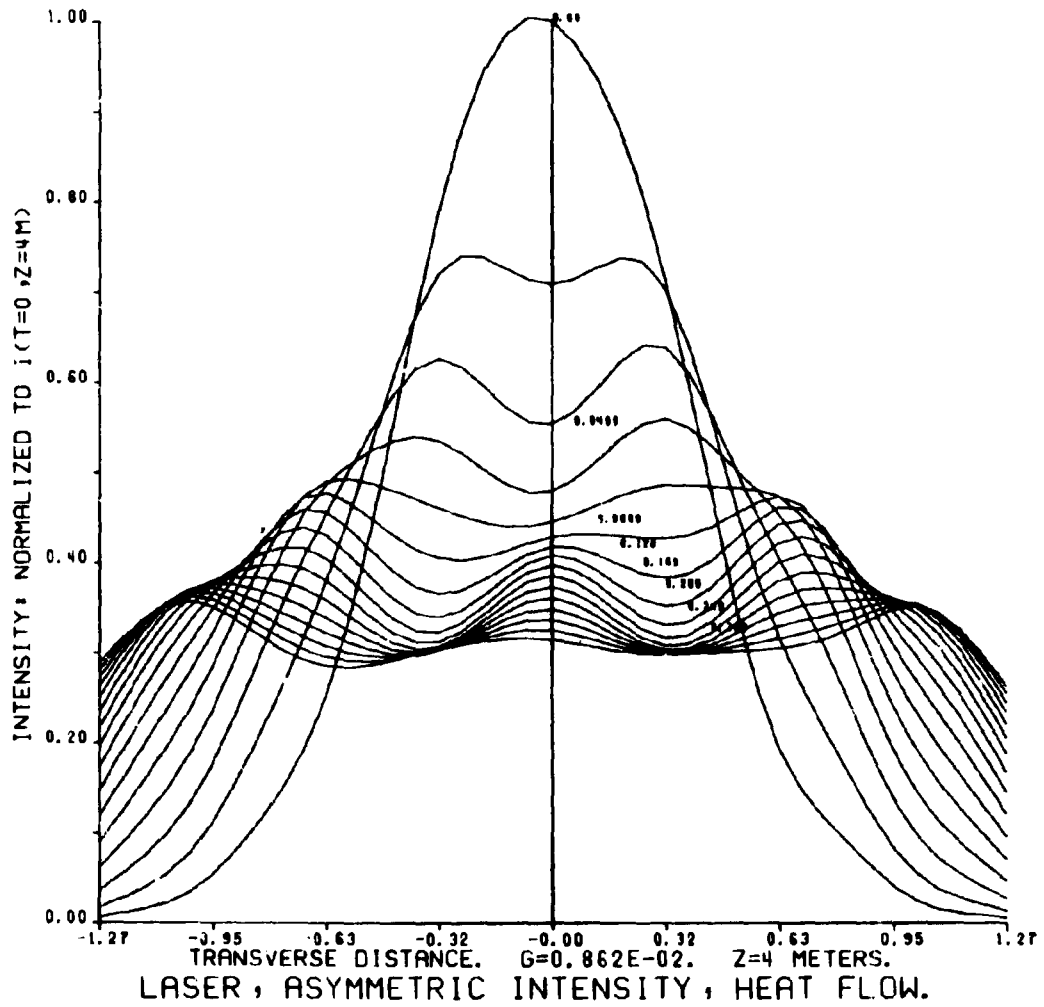


Fig. 5

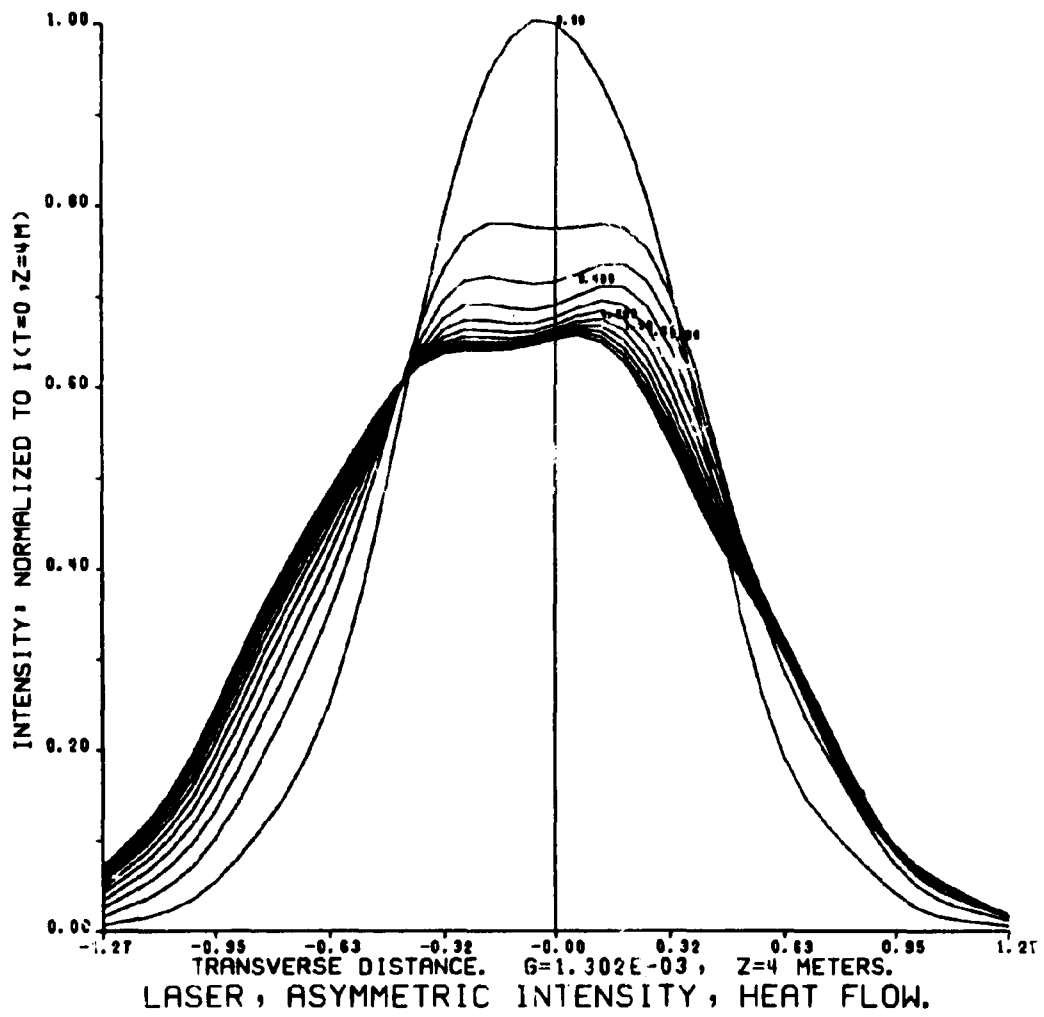


Fig. 6

3. DISCUSSION

The calorimetric absorption measurements on GaAs reported in section f.1 by Steier and Nieh indicate that "naturally" compensated GaAs can have absorbances as low as and, perhaps somewhat lower than, the conventional Cr-doped material. The nature of the impurities which are responsible for the compensation of free carriers in the high resistivity "undoped" material we are working with is unknown. It is hoped that more extensive measurements of the wavelength dependence of the absorption will indicate the extent to which it can be attributed to intrinsic multiphonon processes.

The theoretical expressions for wavelength dependence of the absorption in alkali halides reported in e.1 are in good agreement with experimental data, and seem quite insensitive to the details of the model upon which their derivation is based. The predicted temperature dependence is also insensitive to the model, and could be used (for the alkali halides) to determine whether observed absorbance levels are intrinsic or impurity dominated.

Our numerical simulation of the beam skewing experiments performed by Skolnik at AFCRL reveal appreciable discrepancies among the values of parameters assumed for the window. The magnitude of the observed effect is simply too great to be explained by thermally induced prism effects arising from the measured beam asymmetry. It is possible that the beam asymmetry is a strong function of laser operating power, causing the beam actually employed in the skewing experiment to differ from the lower power beam for which the intensity profile was determined. If the beam skewing effect could be understood and controlled, it could be used for low level absorbance measurements.

The acoustic method for measuring surface properties of IR windows (mentioned in the first quarterly report) was funded at an insignificant level during this period, but preliminary designs have been prepared, and some materials purchased. The technique will be tested first on quartz, for which the problems associated with deposition of acoustical transducers have been solved.

Progress on crystal preparation and window fabrication has been slower than we had hoped, primarily because of the complexity of the required apparatus. All large construction projects are now completed, or nearly so, and we hope to have these areas in full operation by the end of December 1972.

We profited greatly from a visit by A. Kahan from AFCRL during the week of November 13. Drs. H. Posen and A. Armington from AFCRL also visited us during the week of September 11. Drs. Whelan, Shlichta and DeShazer from USC attended the IR Window Conference in Hyannis, Massachusetts during this quarter.

4. SUMMARY

A method is described for measuring minute concentrations of oxygen impurities in GaAs which can be extended to other materials. It involves measuring the oxygen fugacity in a metallic solution before and after dissolving a known amount of the material.

Apparatus for growing ultra pure alkali halides for dopant studies is nearly complete and will probably produce crystals within the next two months. The purification procedure is described. Apparatus for growing ultra pure GaAs is also nearing completion. This facility is important for determination of the origin of residual IR absorption in GaAs.

A hot press utilizing the new technique of solvent assisted compaction has been constructed. The manner in which it is to be used is described in detail.

Mechanical properties of GaAs, including dislocation densities and stress-strain curves have been determined. A new jet polishing technique has been developed for preparing thin foils suitable for electron microscopy.

The I-V characteristic of a Schottky barrier diode deposited on GaAs surfaces was observed to test the quality of surfaces prepared by different polishing techniques. Observed values of the capacitances of MOS structures on these surfaces agree with theoretically expected values.

The abnormal penetration profile of In into CdS and CdTe reported previously is still a mystery despite further experiments. A new value for the lattice constant of CdTe₃ pure and doped, has been found. It implies a density of 5.8555 gm cm⁻³ which is much below the value 6.3 gm cm⁻³ reported in the literature. Other data on the defect chemistry of CdTe are reported.

A theory of the multiphonon contribution to residual IR absorption in ionic materials gives good agreement with the observed frequency dependence of the absorption coefficient. The results are not sensitive to the details of the theoretical model potential employed. Except in Li F, the nonlinear part of the electric dipole moment has been found to have negligible influence on the absorption in the alkali halides. The temperature dependence predicted by this theory is also unaffected by dipole nonlinearities for lattices with small anharmonicities (not Li F.)

Calorimetric measurements of the absorption coefficient of high purity "undoped" GaAs grown at USC have been performed. The material appears to be among the lowest loss GaAs yet reported. With a minimum of about 0.005 cm⁻¹ at $\lambda = 9.28\mu\text{m}$. Repeatable structure in absorbance versus wavelength has been observed.

Numerical simulation of beam slewing experiments performed by Skolnik at AFCRL imply that the observed slew angles are much larger than those expected theoretically. Slews of the observed magnitude could not be obtained even when the beam asymmetry was doubled and the absorption coefficient increased by orders of magnitude.